Benzodithiophene-based Small-molecule Donors for the Next-generation All-Small-Molecule Organic Photovoltaics

Hua Tang[1,2,3 †], Cenqi Yan[3 † *], Jiaming Huang[3], Zhipeng Kan[1], Zeyun Xiao[1], Kuan Sun[4], Gang Li[3,5 *] & Shirong Lu[1 *]

[1] Thin-film Solar Technology Research Center,
Chongqing Institute of Green and Intelligent Technology
Chinese Academy of Sciences, Chongqing, 400714, P. R. China

[2] University of Chinese Academy of Sciences
Beijing 100049, P. R. China

[3] Department of Electronic and Information Engineering,
Research Institute for Smart Energy (RISE), The Hong Kong Polytechnic University, Hung Hom, Kowloon, Hong Kong, P. R. China

[4] Key Laboratory of Low-Grade Energy Utilization Technologies and Systems (Ministry of Education), School of Power Engineering, Chongqing University, Chongqing 400044, P.R. China

[5] Lead Contact

[†]These authors contributed equally to this work.

Correspondent authors: C. Y. (e-mail: cenqi.cq.yan@polyu.edu.hk,) G. L. (e-mail: gang.w.li@polyu.edu.hk) S. L. (e-mail: lushirong@cigit.ac.cn)

Abstract

Solution-processed bulk-heterojunction (BHJ) organic solar cells (OSCs) have considered being a promising candidate for next-generation photovoltaic technology by virtue of their low carbon footprint, short energy payback time, and facile manufacture into light-weight, flexible, and semitransparent products. In this prosperous research field, there is a rising trend of developing and employing all-small-molecule (ASM) OSC due to the distinct merits of small molecules, such as well-defined structures, facile purification, and preeminent batch-to-batch replicability, making it a preferential contender for industrialization. The majority of the best-performing ASM OSCs utilize benzodithiophene (BDT) small molecule donors, and recent breakthroughs demonstrate that the ASM OSCs based on the BDT system has exceeded 15% power conversion efficiency (PCE) mark in the laboratory. This review analyzes the significant study that leads to this remarkable progress and focuses on the most effective BDT small molecule donors. The pivotal structure-property relationships, donor-acceptor matching criteria, and the morphology control approaches are discussed. Last, we summarize the remaining challenges and offer our perspective on the future advance of ASM OSCs.

1. Introduction

Harvesting energy from the sun is a promising solution to supply environmentally-friendly reproducible energy to deal with the issues consequent upon our on-going dependence on fossil fuels.[1-4] Solar cells are considered as devices that convert solar power directly to electricity. The first solar cell was invented in Bell Labs in 1954, followed by persistent efforts in developing this technology for over half a century.[5] Diverse inorganic materials (e. g. silicon and III-V group semiconductors including gallium arsenide (GaAs), copper indium gallium diselenide (CIGS), and cadmium telluride (CdTe))-based solar cells are dominating photovoltaic technologies in the market.[6, 7] Nonetheless, the complicate fabrication process, the costly installation, the non-aesthetic appearance, and the long energy payback time have largely confined the deployment of inorganic photovoltaic technology.[8, 9] To overcome the aforementioned and other technical as well as environmental issues, the researchers have put enormous efforts on pursuing the next-generation photovoltaic technologies.

Solution-processed bulk-heterojunction (BHJ) organic solar cells (OSCs) have emerged to be a potential contender for next-generation photovoltaic technology by right of their advantages, such as low carbon footmark, low-temperature processing, short energy payback period and facile manufacture into flexible, light-weight, and semitransparent products.[4, 6, 10-18] Unlike inorganic solar cells, mainly concentrating on the solar farm market, OSCs also pay close attention to the building-integrated PV and indoor application market, which has the capacity to power the Internet of things ecosystem, involving remote and distributed actuators, sensors and communication units, such as smartphones, smartwatches, and intelligent robots.[19] In the 1970s, several conductive organic materials were found to exhibit the photovoltaic effect and drew considerable attention from the scientific community.[2, 20] Later in 1986, Tang reported the bilayer OSC, which presented a power conversion efficiency (PCE) $<$1% but established the foundation of the donor/acceptor OSC device architecture.[21] In 1995, the BHJ OSC was invented to further improve the PCE. Meanwhile, efficient fullerene electron acceptor materials were introduced to the organic photovoltaic field, which shifted the research focus to polymeric donor materials.[22] Subsequent advances involving novel polymeric donors have continued to set new PCE records.[4, 6, 20, 23, 24] However, polymers typically suffer from undefined molecule structure and batch to batch variation, which largely impedes the industrialization of polymer-based OSCs.[25-29]

All-small-molecule (ASM) OSCs appear as a preferred solution for industrialization, enabled by their good scalability which is derived from well-defined molecule structures, facile purification, and preeminent batch-to-batch reproducibility of ASM OSCs.[29-32] Benzodithiophene (BDT) donor-based devices dominate the majority of the high-performing OSCs. For instance, BDT in polymer donors has enabled the enormous success of PTB family OSCs.[15, 33-38] In 2011, the BDT unit was first introduced into small molecule donors, and subsequent development has resulted in a family of BDT based high-performance small molecule donors.[31, 39] In 2014, ASM OSCs based on BDT-based donor and fullerene acceptor have obtained nearly 10% PCE,[40] and the invention of nematic liquid crystalline BDT-based donor BTR obtained a PCE of 9.3% with thick film (*ca*. 300 nm) active layer, important to future industrialization.[41] The advances of design for BDT-based small molecule donors and nonfullerene acceptors (NFAs) continuously promote the progress of ASM OSCs and break the PCE record values repeatedly. In 2020, the state-of-the-art ASM OSCs based on BTR derivative (B1) (**Figure 5**) and the derivative of star NFA Y6[42] have exceeded the PCE mark of 15%, typically believe to be threshed for industrialization.[43] A brief timeline of significant breakthroughs in BDT donor-based ASM OSC is presented in **Figure 1**.[20, 21, 40-45]

In this review, we first introduce the primary working mechanism of OSCs. Second, we summarize the key progress of the design and synthesis of BDT-based small molecule donors and analyze their structure-property-performance relationship. We then discuss a few aspects involving device physics, morphology control approach, and ternary strategy. Finally, we summarize the remaining challenges and offer our perspective on the future advance of ASM OSCs.

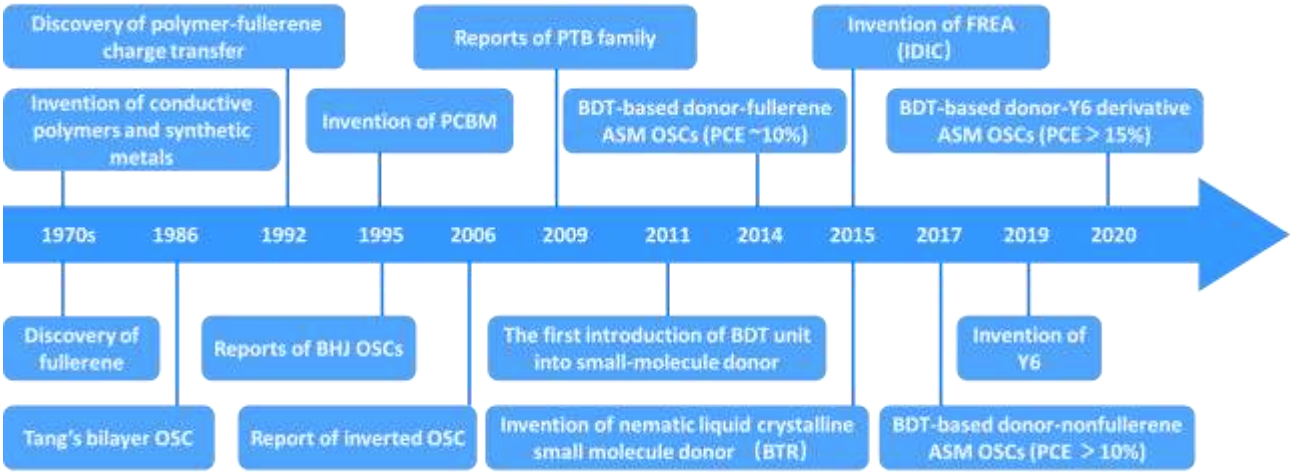

Figure 1. A brief timeline of the development of BDT donor-based ASM OSCs. The advances depicted in the cells are several milestones in the advance of BDT donor-based ASM OSCs & OSCs in general.

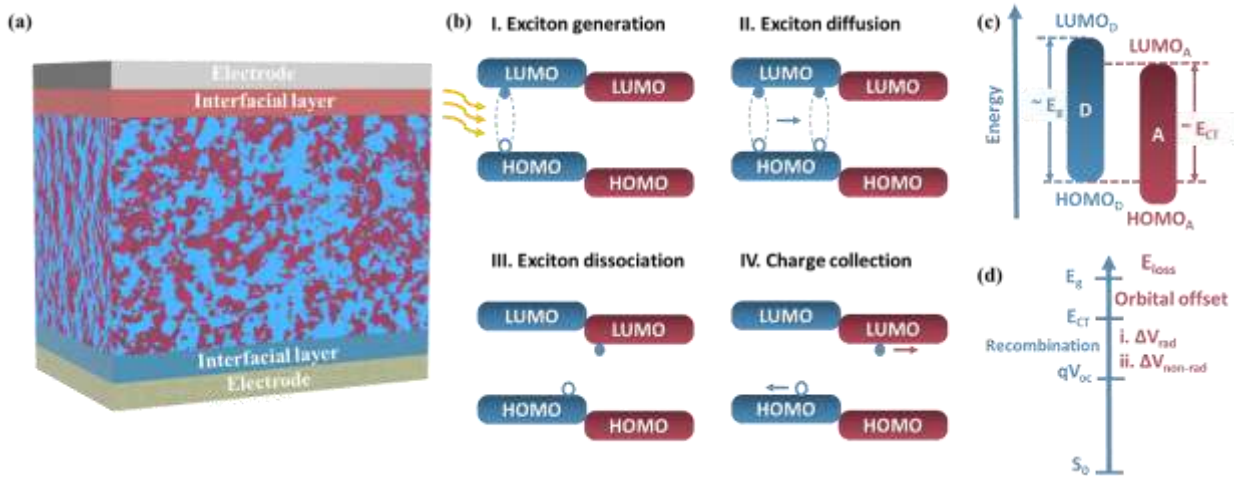

Figure 2. (a) The architecture of a BHJ OSC. In an ideal BHJ device architecture, donor and acceptor materials shape nanoscale phase separation and construct bicontinuous interpenetrating networks with large donor-acceptor interfacial areas. The blue and red areas represent the donor and acceptor domains, respectively. Interfacial layers in the device architecture are employed as charge-transport layers, charge-blocking layers, and optical spacers, which can build ohmic contacts between the electrode and active layer. (b) Schematic revealing the working principle of OSCs. (c) Orbital energy diagram for a typical donor-acceptor pairing. The optical energy gap of the blend refers to the smaller optical energy gap of the donor or acceptor. The CT state energy can be summarized as the difference between the LUMO of the acceptor and the HOMO of the

donor. E_g: optical energy gap; E_{ct}: charge-transfer state energy. (d) Energy loss for OSCs can be divided into charge generation (E_g - E_{ct}) and charge recombination (E_{ct} - qV_{OC}). Charge recombination energy loss results from both radiative and non-radiative CT state decay. S_0: ground state.

2. Operating Principle of Organic Solar Cells

OSCs are devices that contain organic materials for solar radiation absorption and carrier transport to deliver electricity from sunlight via the photovoltaic effect. Generally, OSCs are based on blends of an electron-rich ((‘donor’, D)) material and an electron-poor (‘acceptor’, A) material that forms BHJs in devices.[20] Donor and acceptor possess different frontier molecule orbitals, and the energy difference between the highest occupied molecular orbital (HOMO) and the lowest unoccupied molecular orbital (LUMO) determines the bandgap (E_g) of the materials. The working principle of OSCs involves four key steps: (i) solar radiation absorption and exciton generation (The strongly bound excitons are generated on account of the low dielectric constant of organic semiconductors); (ii) exciton diffusion to the D/A interface; (iii) formation of a charge-transfer (CT) complex, followed by dissociation into free charge carriers at the interface; (iv) charge transport and collection. Every step is vital to deliver the PCE of OSCs.

The PCE of OSCs is given by:

$$PCE = V_{OC} J_{SC} FF / P_{in}$$

Where P_{in} represents the power density of the incident solar energy, V_{OC} is the open-circuit voltage, J_{SC} is the short-circuit current density, FF is the fill factor (defined as $P_{max} / V_{OC} J_{SC}$), where P_{max} is the maximum power density. The V_{OC} is usually dominated by the energy difference between the LUMO of the acceptor and the HOMO of the donor. Recent progress has shown that V_{OC} is also affected by other factors, including the driving force for charge separation, the unavoidable radiative recombination, and the existence of energetic tail and trap states.[46, 47] These factors result in the energy loss (E_{loss} = Eg - eV_{OC} where Eg refers to the smaller optical bandgap of the donor or acceptor. J_{SC} is limited by the efficiency of exciton generation, exciton dissociation, charge carrier transport, and collection. FF is mainly interrelated with the competition between charge extraction and recombination, both of which have a nonlinear growth relationship with the mobilities of charge carriers.[48-52] To achieve excellent PCE, it is of

importance to maximize the product of the three parameters, V_{OC}, J_{SC}, and FF, which requires the match of donors and acceptors, and the reasonable nanoscale phase separation to simultaneously retain efficient charge generation while reducing recombination.

A few years ago, particularly prior to 2017, most of ASM OSCs have employed fullerene acceptors, mainly [6,6]-phenyl-C61-butyric acid methyl ester ($PC_{61}BM$) and [6,6]-phenyl-C71-butyric acid methyl ester ($PC_{71}BM$). ASM OSCs based on BDT-based small molecule donor: fullerene acceptors achieved PCEs of up to 11%, mainly ascribed to high electron mobilities and excellent interpenetrating D/A networks in the BHJ active layer.[53, 54] However, several notable drawbacks, such as weak absorption in the visible and near-infrared (NIR) regions, limited tunability of energy levels, the high driving force (~ 0.3 eV) for charge separation, photochemical and thermal instability as well as a time-consuming purification process. These factors result in a trade-off between high photocurrent and small voltage loss and largely confine the advance of fullerene-based ASM OSCs.[32, 55, 56] On the other hand, together with the surprising progress in NFAs in polymer OSCs, the ASM OSCs research community naturally shift the focus to NFA-based ASM OSCs. NFAs possess tunable energy level and strong and complementary absorption profile relative to wide/medium bandgap BDT-based small molecule donors, small (even negligible) driving energy for charge separation and easy modification of chemical structures, crystallinity and phase separation, leading to the possibility of simultaneously achieve high J_{SC} and V_{OC}. Currently, the BDT-based small molecule donor: NFA ASM OSCs have broken the PCE record repeatedly, and the scientific community has been making tremendous efforts in molecule design, device engineering, device physics, and theoretical modeling, towards the industrialization of the next generation photovoltaic technology.[1, 2, 4, 7, 31, 39]

3. BDT-based small molecule donors

The advances of ASM OSCs are inseparable with the sustaining innovation of small molecule donor materials. Many electron-donating cores are proven effective to construct ASM OSCs, including BDT, oligothiophene, naphthodithiophene (NDT), dithienosilole (DTS) and porphyrin.[31, 39] In terms of PCEs, the BDT-based small molecule donors are the most promising. Currently, the BDT-based small molecule donors have achieved 15.3% efficiency[43], outcompeting its counterparts based on oligothiophene (11.45%),[57] NDT (10.7%),[58] DTS

(8.2%)[59] and porphyrin (12.08%).[49] The BDT-based small molecule donors consist of BDT electron-donating core and electron-withdrawing end groups (EGs), and in some cases π-conjugated bridges. Chemical modifications of these donors endow them with highly tunable molecular structures, planarity, molecular packing, morphology, and optoelectronic properties. Modifications can be applied to cores, side chains, EGs, and π-conjugated bridges to enhance the photovoltaic performance of BDT-based small molecule donors.

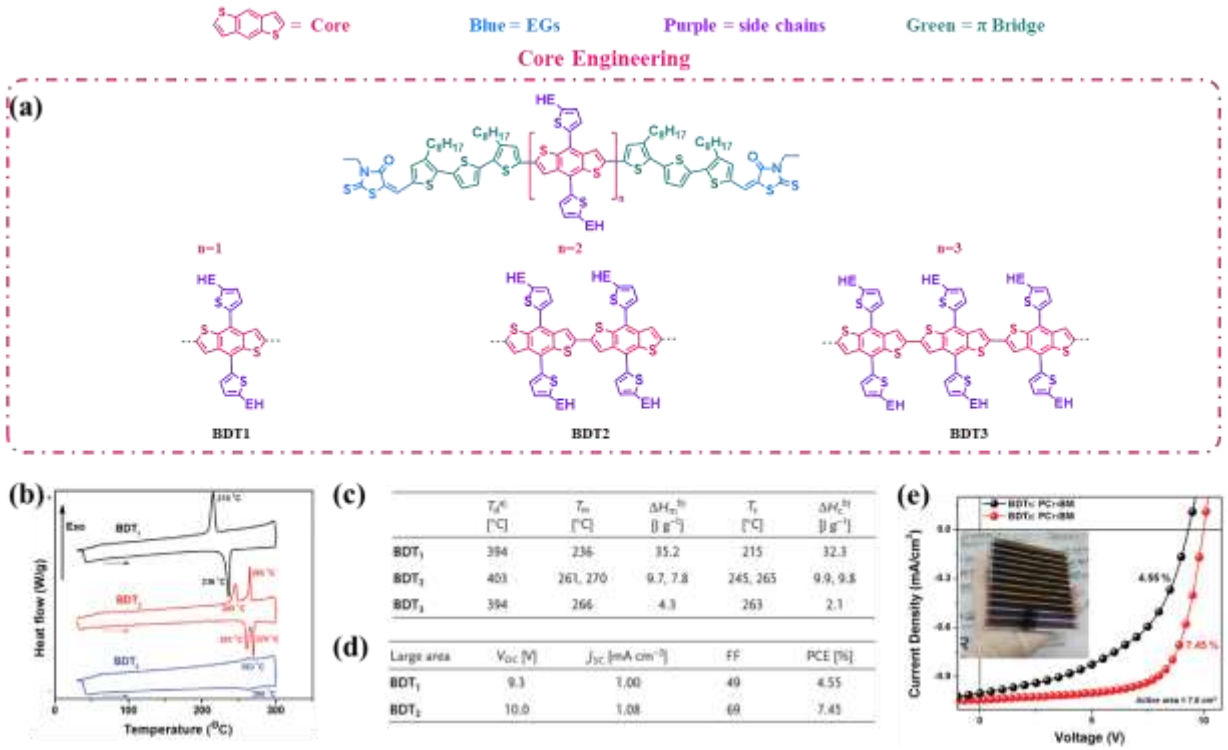

	$T_d^{a)}$ [°C]	T_m [°C]	$\Delta H_m^{b)}$ [J g^{-1}]	T_c [°C]	$\Delta H_c^{b)}$ [J g^{-1}]
BDT_1	394	236	35.2	215	32.3
BDT_2	403	261, 270	9.7, 7.8	245, 265	9.9, 9.8
BDT_3	394	266	4.3	263	2.1

Large area	V_{OC} [V]	J_{SC} [mA cm^{-2}]	FF	PCE [%]
BDT_1	9.3	1.00	49	4.55
BDT_2	10.0	1.08	69	7.45

Figure 3. (a) The molecule structure evolvement of BDT-based small-molecule donors via core engineering. (b) The second heating DSC thermograms of BDT1, BDT2, and BDT3 at a heating rate of 10 ℃ min^{-1}. (c) The thermal data of BDT1, BDT2, and BDT3. (d) The photovoltaic parameters in a large area (77.8 cm^2) and (e) the corresponding *J*-*V* curves of the optimized BDT1: $PC_{71}BM$ and BDT2: $PC_{71}BM$ devices. Reproduced with permission.[60] Copyright 2016, Wiley-VCH.

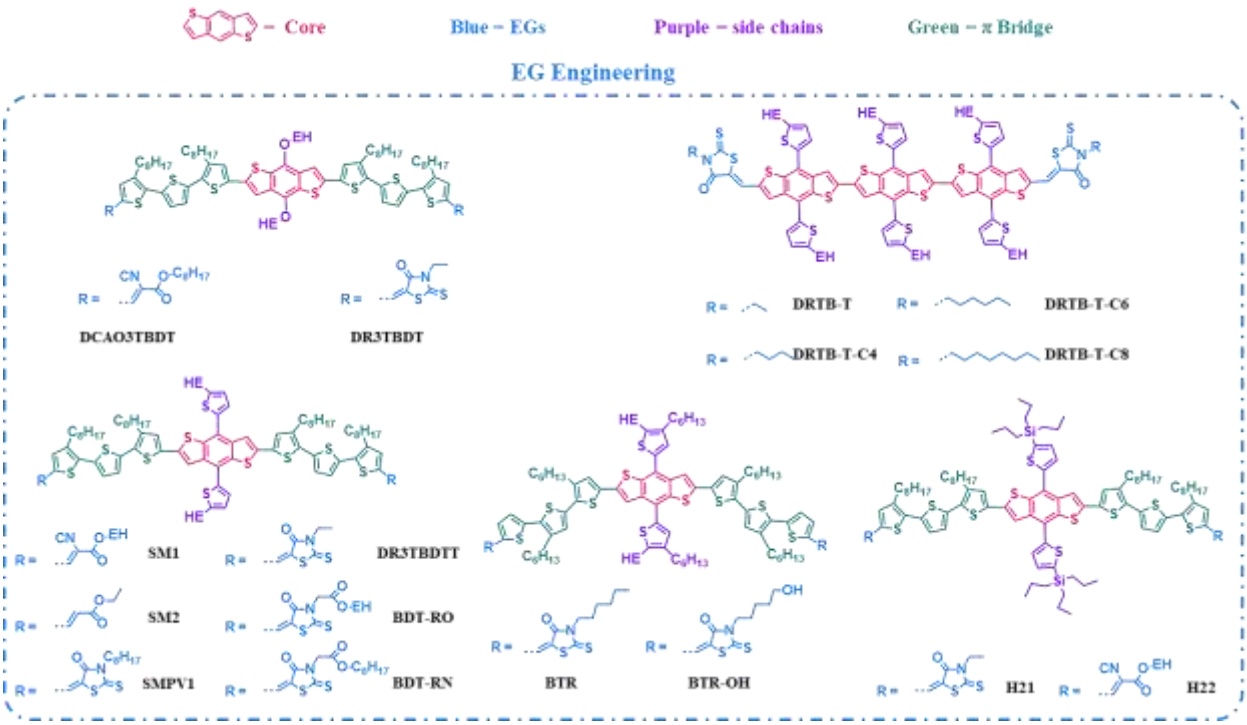

Figure 4. (a) The molecule structure evolvement of BDT-based small-molecule donors via EG engineering.

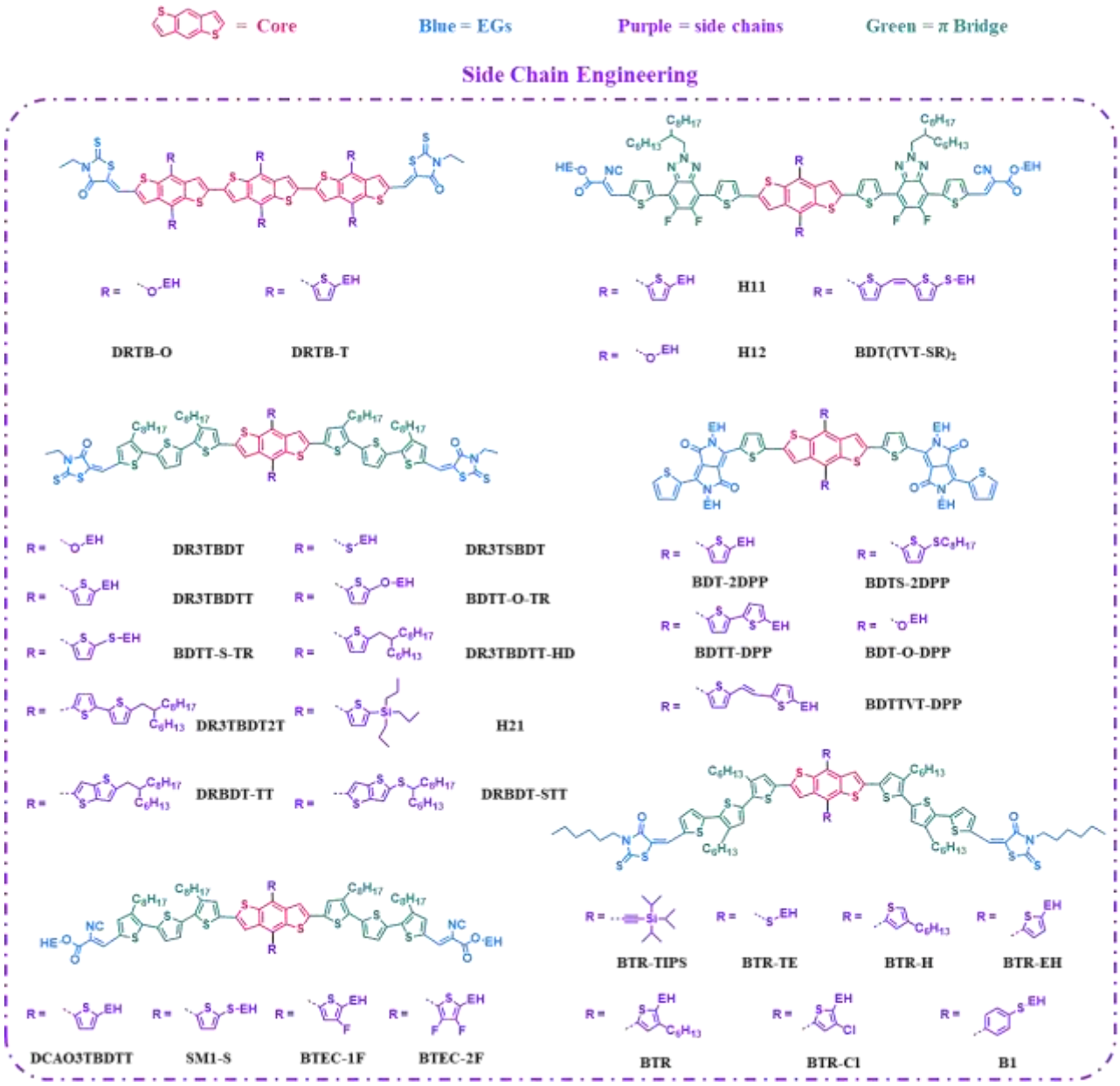

Figure 5. The molecule structure evolvement of BDT-based small molecule donors via side-chain engineering.

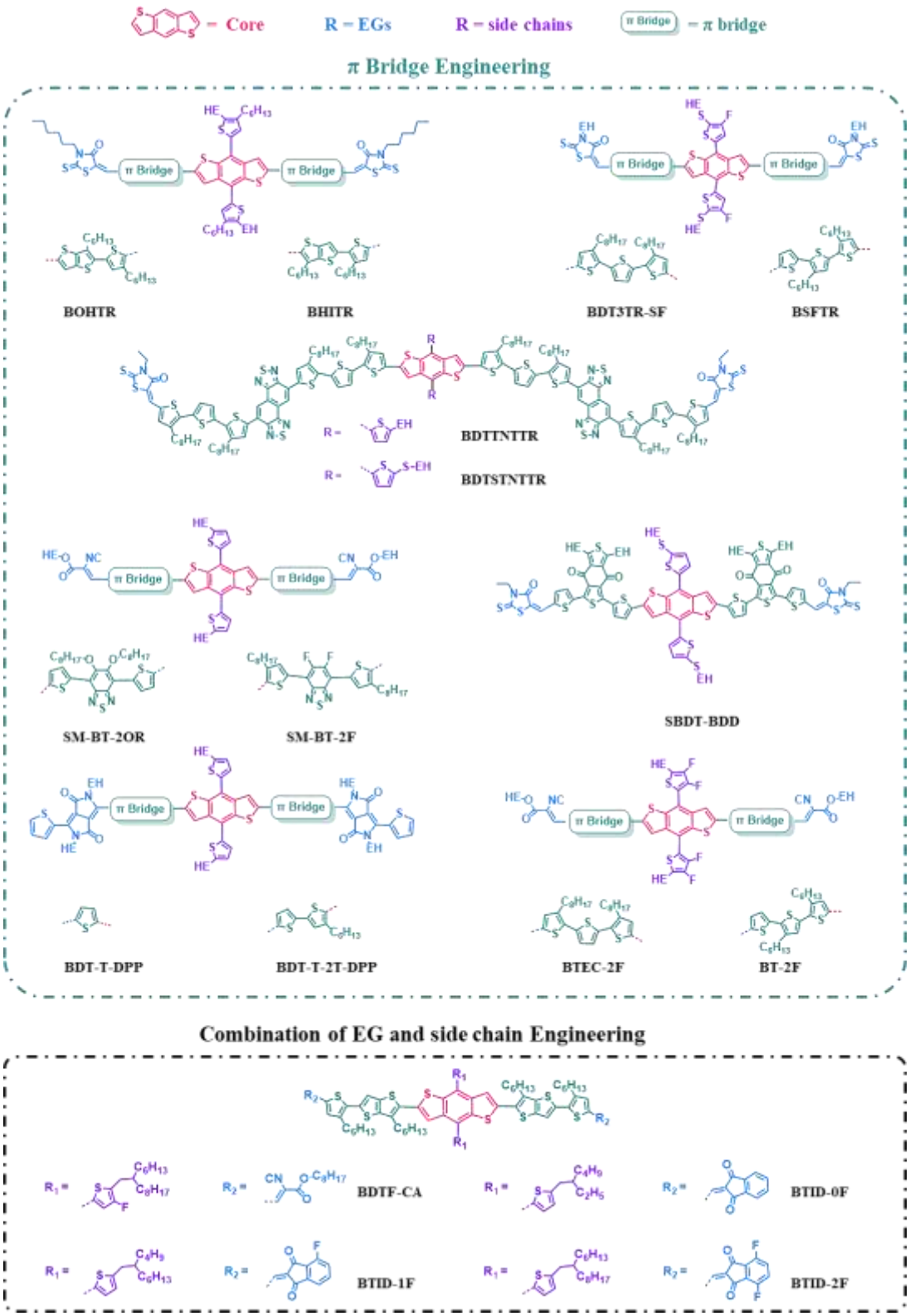

Figure 6. The molecule structure evolvement of BDT-based small molecule donors via π bridge engineering and combination of EG and side-chain engineering.

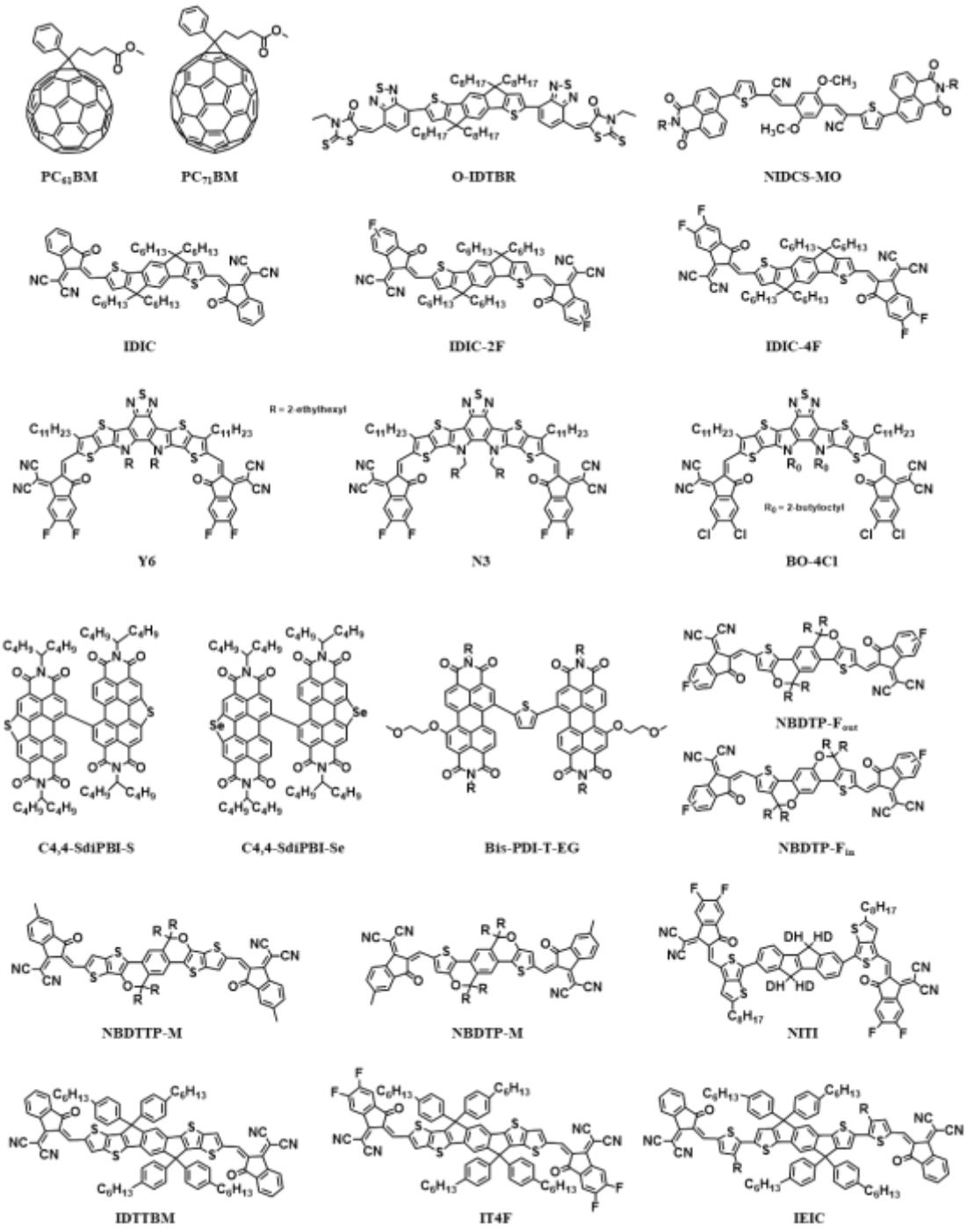

Figure 7. The molecule structures of the small molecule acceptors discussed in the review.

Table 1. Optoelectronic properties and device parameters for BDT small molecule donor-based ASM OSCs.

Donor	λ_{max} [nm]	*HOMO/LUMO [eV]*	E_g [eV]	μ_h [$cm^2 V^{-1} s^{-1}$]	Acceptor	V_{OC} [V]	J_{SC} [mA cm^{-2}]	FF [%]	PCE [b] [%]	Ref
BDT1	590	-5.14/-3.37	1.77	5.38×10^{-5}	$PC_{71}BM$	0.89	13.02	62	7.18	[60]
BDT2	580	-5.13/-3.37	1.76	2.44×10^{-4}	$PC_{71}BM$	0.89	13.17	73	8.56	[60]
BDT3	520	-5.10/-3.28	1.82	9.19×10^{-5}	$PC_{71}BM$	0.90	11.34	70	7.14	[60]
DRTB-T (BDT3TR)	582	-5.48/-3.56	1.90	3.74×10^{-7}	$PC_{71}BM$	1.01	10.02	70	7.08	[61]
				3.46×10^{-4}	IDIC	0.98	14.22	65	9.06	[61]
				1.88×10^{-4}	IT4F	0.89	16.66	64	9.52	[62]
				/	O-IDTBR	1.06	12.10	55	6.96	[63]
DRTB-T-C4	/	-5.50/-3.32	1.97	4.81×10^{-4}	IT4F	0.91	18.27	68	11.24	[62]
DRTB-T-C6	/	-5.50/-3.32	1.97	2.95×10^{-4}	IT4F	0.93	17.92	63	10.52	[62]
DRTB-T-C8	/	-5.52/-3.33	1.97	1.46×10^{-4}	IT4F	0.93	16.15	61	9.14	[62]
DRTB-O	572	-5.50/-3.56	1.90	5.44×10^{-5}	$PC_{71}BM$	1.01	7.49	65	4.91	[61]
				1.14×10^{-4}	IDIC	0.99	0.57	27	0.15	[61]
SM1	566	-5.24/-2.82	1.88	1.60×10^{-4}	IDIC	0.91	15.18	73.55	10.11	[64]
SM2	521	-5.04/-2.70	2.02	1.47×10^{-4}	IDIC	0.77	10.77	64.40	5.32	[64]
DR3TBDTT	591	-5.02/-3.27	1.72	2.88×10^{-4}	$PC_{71}BM$	0.93	13.17	66.3	8.12	[27]
					$PC_{71}BM$	0.93	12.97	62.97	7.61	[27]
				3.81×10^{-4}	C4,4-SdiPBI-S	0.91	11.12	57.32	5.81	[65]
				4.78×10^{-4}	C4,4-SdiPBI-Se	0.92	11.55	58.72	6.22	[65]
				/	O-IDTBR	1.12	11.3	50	6.4	[66]
				4.78×10^{-5}	IDIC	0.86	14.39	61.19	7.61	[67]
SMPV1	584	-5.51/-3.64	1.77	3.3×10^{-4}	$PC_{71}BM$	0.94	12.17	70.4	8.02	[68]
BDT-RO	580	-5.05/-3.30	1.75	3.24×10^{-4}	IDIC	0.88	15.37	66.56	9.01	[67]
BDT-RN	580	-5.05/-3.30	1.75	1.87×10^{-4}	IDIC	0.87	14.85	64.88	8.36	[67]
H21	582	-5.38/-3.63	1.81	2.49×10^{-4}	IDIC	0.90	13.00	65.58	7.62	[69]
H22	560	-5.39/-3.59	1.89	4.26×10^{-4}	IDIC	0.94	15.38	71.15	10.29	[69]
$DCAO_3TBDT$	560	-5.04/-3.24	1.84	1.38×10^{-4}	$PC_{61}BM$	0.95	8.00	60.0	4.56	[30]
				/	$PC_{71}BM$	0.93	3.74	60.1	2.09	[30]
DR3TBDT	583	-5.02/-3.27	1.74	/	$PC_{61}BM$	0.91	10.78	65.0	6.38	[30]

				2.47×10^{-4}	$PC_{71}BM$	0.93	12.21	65.0	7.38	[30]
H11	/	-5.31/-3.03	1.87	7.7×10^{-5}	IDIC	0.98	15.21	65.46	9.73	[56]
H12	/	-5.28/-3.01	1.87	7.9×10^{-5}	IDIC	0.96	10.51	54.89	5.51	[56]
$BDT(TVT\text{-}SR)_2$	558	-5.33/-3.18	1.82	1.48×10^{-4}	IDIC	0.98	15.92	71.15	11.10	[70]
BDT-2DPP	626	-5.23/-3.46	1.65	3.0×10^{-3}	IEIC	0.90	8.24	54	4.00	[71]
BDTS-2DPP	624	-5.28/-3.49	1.65	1.1×10^{-2}	IEIC	0.94	10.87	59	6.03	[71]
BDTTT-DPP	618	-5.04/-3.46	1.69	1.5×10^{-3}	$PC_{61}BM$	0.83	10.92	61.05	5.53	[72]
				2.0×10^{-4}	IDIC	0.81	10.16	58.28	4.80	[72]
BDTTVT-DPP	628	-5.07/-3.43	1.67	7.2×10^{-4}	$PC_{61}BM$	0.83	7.32	57.28	3.48	[72]
				4.7×10^{-4}	IDIC	0.82	11.30	59.17	5.48	[72]
DR3TSBDT	586	-5.07/-3.30	1.74	6.13×10^{-4}	$PC_{71}BM$	0.91	14.45	73	9.95	[40]
BDTT-TR (DR3TBDTT)		-5.17/-3.39	1.74	5.48×10^{-4}	$PC_{71}BM$	0.93	11.75	68.1	7.44	[73]
BDTT-O-TR	582	-5.14/-3.34	1.74	3.70×10^{-4}	$PC_{71}BM$	0.90	11.03	65.5	6.50	[73]
BDTT-S-TR	588	-5.18/-3.25	1.73	8.51×10^{-4}	$PC_{71}BM$	0.97	13.45	70.5	9.20	[73]
				5.51×10^{-5}	NIDCS-MO	0.97	9.12	60.3	5.33	[74]
DR3TBDTT-HD	589	-5.06/-3.29	1.76	1.52×10^{-4}	$PC_{71}BM$	0.96	11.92	59.4	6.79	[27]
DR3TBDT2T	591	-5.07/-3.29	1.76	3.29×10^{-4}	$PC_{71}BM$	0.92	12.09	72.1	8.02	[27]
DRBDT-TT	589	-5.13/-3.33	1.78	5.41×10^{-4}	$PC_{71}BM$	0.91	12.93	71	8.70	[75]
DRBDT-STT	584	-5.15/-3.34	1.80	4.74×10^{-4}	$PC_{71}BM$	0.90	12.20	70	8.01	[75]
BTR	578	-5.34/-3.52	1.82	1.6×10^{-3}	$PC_{71}BM$	0.90	13.90	74	9.3	[41]
				3.01×10^{-4}	Y6	0.85	22.25	56.4	10.67	[76]
				1.4×10^{-3}	BO-4Cl	0.83	18.93	72	11.3	[43]
BTR-Cl	580	-5.46/-3.70	1.78	2.72×10^{-4}	Y6	0.86	24.17	65.5	13.61	[76]
BTR-OH	574	-5.49/-3.45	1.82	1.4×10^{-5}	$PC_{71}BM$	0.90	13.56	65.3	8.00	[77]
BTR-TIPS	570	-5.42/-3.13	1.84	2.8×10^{-4}	$PC_{71}BM$	0.94	8.60	64	5.20	[78]
BTR-TE	582	-5.39/-3.33	1.78	9.4×10^{-4}	$PC_{71}BM$	0.90	14.15	72	9.15	[78]
BTR-H	593	-5.32/-3.29	1.76	3.9×10^{-4}	$PC_{71}BM$	0.87	10.30	60	5.30	[78]
BTR-EH	594	-5.32/-3.34	1.73	7.2×10^{-4}	$PC_{71}BM$	0.89	12.00	69	7.40	[78]
B1	/	-5.37/-3.51	/	2.3×10^{-3}	BO-4Cl	0.83	25.27	73	15.3	[43]
DCAO3TBDTT	567	-5.25/-3.33	/	4.60×10^{-4}	Y6	0.80	21.71	60.95	10.64	[79]
BTEC-1F	561	-5.37/-3.37	/	4.17×10^{-4}	Y6	0.87	21.21	61.35	11.33	[79]

BTEC-2F	561	-5.39/-3.38	/	5.18×10^{-4}	Y6	0.85	21.55	72.35	13.34	[79]
BIHTR	571	-5.40/-3.27	1.79	1.69×10^{-3}	Y6	0.84	21.5	68.4	12.3	[80]
BOHTR	569	-5.36/-3.24	1.76	1.68×10^{-3}	Y6	0.83	23.1	56.2	10.8	[80]
BDT3TR-SF	564	-5.37/-2.85	1.81	1.80×10^{-4}	NBDTP-F_{out}	0.80	21.40	64.6	11.02	[81]
				1.39×10^{-4}	NBDTTP-M	1.01	5.11	55.7	2.89	[82]
				1.92×10^{-4}	NBDTP-M	0.97	16.42	64.3	10.23	[82]
BSFTR	568	-5.59/-3.61	1.83	6.43×10^{-4}	Y6	0.85	23.16	69.66	13.69	[83]
				3.38×10^{-4}	NBDTP-F_{out}	0.80	21.69	70.93	12.26	[84]
				/	NBDTP-M_{out}	0.95	13.99	67.31	8.94	[84]
				/	IDIC	0.98	9.30	70.88	6.43	[84]
BDTTNTTR	/	-5.29/-3.53	1.51	2.01×10^{-3}	$PC_{71}BM$	0.89	15.70	71.7	10.02	[54]
BDTSTNTTR	/	-5.35/-3.60	1.50	3.18×10^{-3}	$PC_{71}BM$	0.93	16.21	76.5	11.53	[54]
SM-BT-2OR	584	-5.34/-3.12	1.77	7.37×10^{-5}	IDIC	0.94	13.57	56.5	7.20	[85]
SM-BT-2F	606	-5.36/-3.26	1.66	1.77×10^{-5}	IDIC	0.98	6.74	41.7	2.76	[85]
BT-2F	554	-5.40/-3.40	/	3.93×10^{-4}	Y6	0.85	22.38	72.27	13.80	[86]
				/	N3	0.84	23.81	70.22	14.09	[86]
BDT-O-DPP	618	-5.13/-3.65	/	1.1×10^{-3}	Bis-PDI-T-EG	0.95	3,46	41	1.34	[87]
BDT-T-DPP	629	-5.15/-3.44	/	2.2×10^{-2}	Bis-PDI-T-EG	0.92	4.66	47	2.01	[87]
BDT-T-2T-DPP	620	-5.20/3.64	/	1.6×10^{-3}	Bis-PDI-T-EG	0.83	4.60	43	1.62	[87]
SBDT-BDD	581	-5.25/-3.55	1.77	8.1×10^{-4}	$PC_{71}BM$	0.99	12.82	66.3	8.1	[88]
				3.5×10^{-4}	IDIC	0.97	15.15	62.5	9.2	[88]
BDTF-CA	561	-5.44/-3.53	1.90	5.4×10^{-5}	IDIC	0.99	12.09	51.14	6.12	[89]
				1.9×10^{-4}	IDIC-2F	0.94	16.69	58.07	9.11	[89]
				6.3×10^{-4}	IDIC-4F	0.88	14.96	63.95	8.42	[89]
BTID-0F	/	-4.91/-3.20	1.71	1.4×10^{-3}	$PC_{71}BM$	0.93	14.0	64.0	8.30	[53]
BTID-1F	/	-4.98/-3.28	1.70	6.4×10^{-4}	$PC_{71}BM$	0.94	15.3	72.0	10.4	[53]
BTID-2F	/	-5.05/-3.37	1.68	4.7×10^{-4}	$PC_{71}BM$	0.95	15.7	76.0	11.3	[53]
				8.72×10^{-5}	IDIC	0.90	13.98	65.20	8.23	[90]

λ_{max}, the absorption maximum of donors' pristine films.

HOMO/LUMO, measured or estimated using various techniques and with different assumptions; the values should be compared with caution and regarding the original papers.

E_{op}, optical bandgap.

μ_h, hole mobility of BHJ active layers measured by the space-charge-limited current (SCLC) method.
V_{OC}, open-circuit voltage; J_{SC}, short-circuit current density; FF, fill factor; PCE, power conversion efficiency. (The donor: acceptor ratios, processing conditions (including additives), and device structures may be varied in different research works. Accordingly, values from different studies are often not directly comparable.)

3.1 Effect of the Core.

Core moieties are of significance for constructing an efficient acceptor-donor-acceptor (A – D – A or A – π – D – π – A) push-pull structure. In which, BDT building block is the dominant electron-donating core. Several efficient cores, such as DTS and cyclopentadithiophenes (CPDT) are evolved from the BDT unit and also obtained excellent PCEs. In this concise review, we only concentrate on the purely BDT based small-molecule donors.

One way is to change the number of BDT electron-donating units. Encouraged by the success of DRCN5T and DRCN7T featuring a five-thiophene and seven-thiophene core[25, 28], Lee and co-workers first demonstrated a series of BDT-based small molecule donors (BDT1, BDT2, and BDT3) bearing 1 to 3 BDT units[60] (**Figure 3a**). BDT_1 exhibited the melting temperature (Tm) of 236 °C (ΔH_m = 35.2 J g^{-1}) and the recrystallization temperature (Tc) of 215 °C (ΔH_c = 32.3 J g^{-1}) (**Figure 3 b-c**), respectively. They are nearly identical to those for six-thiophene oligomers demonstrated by Chen and co-workers[28], indicating interaction with the oligothiophene units contributes a lot to the crystallization of BDT1. ΔH_m and ΔH_c of the small molecule donor gradually declined with the increasing number of BDT units, probably on account of the diminished impact of the oligothiophene-unit-driven molecular ordering. BDT2 presented two different T_m values at 261 °C (ΔH_m = 9.7 J g^{-1}) and 270 °C (ΔH_m = 7.8 J g^{-1}) (**Figure 3 b-c**), indicating that the highly coplanar structure by two BDT units results in the co-existence of two clear crystalline phases. Thus, BDT2 has fewer crystalline amounts but larger intermolecular interaction than BDT1. By comparison, BDT3 only demonstrated a weak single-phase transition with a T_m of 266 °C, still much higher than BDT1, indicative of the existence of a strong intermolecular interaction between BDT units. Meanwhile, the lowest ΔH_m value of BDT3 indicates the weakest impact of the oligothiophene-driven molecular ordering. Such strong intermolecular interactions in BDT2 produced the desired interconnected structure in the BHJ film, which enhanced exciton diffusion and charge transport. Consequently, BDT2 delivers a PCE of 8.56% with a FF of 73% in small-area ASM OSC, and 7.45% efficiency in a rigid module of 77.8 cm^2, outperforming BDT1 and BDT3.[60] (**Figure 3 d-e**)

3.2 Effect of the EG.

The choice of EGs generally affects the optical and electrochemical properties, as well as morphological factors of small molecule donors.[39] So far, only a few EGs have been developed and used in small-molecule donors, among which, the 3-ethylrhodanine EG is the most dominant selection.[31]

Chen and co-workers designed and synthesized two small-molecule donors, namely $DCAO_3TBDT$ and DR3TBDT, which possesses 2-ethylhexoxy substituted BDT core, dioctyltert-thiophene spacer, and octyl cyanoacetate and 3-ethylrhodanine end groups, respectively. The introduction of 3-ethylrhodanine terminus significantly improved the photon absorption, leading to the much higher J_{SC} of DR3TBDT: $PC_{71}BM$ system than that of DCAO3TBDT: $PC_{71}BM$ (**Figure 4**). Consequently, DR3TBDT: $PC_{71}BM$ blend demonstrated a remarkably enhanced PCE of 7.38% relative to $DCAO_3TBDT$: $PC_{71}BM$ (2.09%).[30] (**Table 1**)

In the past decade, rhodanine EG based small molecule donors have reached the record PCE values repeatedly, and thus the modification on rhodanine EG can be an effective strategy to elevate the PCEs of ASM OSCs further. One of us, Li, Yang, and coworkers designed two-dimensional (2D) BDT based small molecule donors, SMPV1, by replacing the 3-ethylrodanine end-group in DR3TBDTT with 3-octylrodanine terminus. The longer chains work to improve solubility and film quality. Moreover, the longer octyl chains blue-shifted the absorption profile, down-shifted the energy level, and enhanced the hole mobility of SMPV1, thus successfully improving the certified PCEs of ASM OSCs from DR3TBDTT: $PC_{71}BM$ (7.61%) to SMPV1: $PC_{71}BM$ (8.02%)[68]. (**Table 1**) Hou and co-workers also employed such strategy and designed a group of alkylthienyl-substituted BDT trimers named DRTB-T-CX which differs in end-group alkyl chains (**Figure 4, Table 1**).[61 62] Along with the extending lengths of the alkyl chain of EGs, the small molecule donor demonstrated nearly the identical photoelectric properties but varied molecule orientation. As the 2D GIWAXS pattern showed, DRTB-T-C2 showed a typical edge-on molecular orientation with lamellar packing diffraction in the out-of-plane (OOP) direction and π-π stacking diffraction in the In-plane (IP) direction. DRTB-T-C4 presented a preferred face-on feature with π-π stacking mostly in the OOP direction; the π-π peak localizes at directions roughly 60° with respect to the substrate in DRTB-T-C6 pristine film; and face-on orientation dominates in DRTB-T-C8 film. In IT-4F based blend film, the face-on fraction has a positive correlation the length of alkyls on the rhodanine EG of donors. The special decline in the face-

on ratio of DRTB-T-C6 owing to the formation of the favorable orientation at approximately 30° relative to the substrate. Besides, the C4 system has a much smaller domain size than the DRTB-T-C8 system, which increased the D/A interfacial area and thus enhanced exciton dissociation efficiency. In the solid-state, the face-on orientation is capable of simultaneously increasing the coherence length (CCL) of π - π stacking and enhancing the charge mobilities, leading to the DRTB-T-C4: IT-4F with a champion PCE of 11.24%.[62] It is noteworthy that, even at a high active-layer thickness of 300 nm, devices based on DRTB-T-C4: IT-4F still retain an excellent PCE of 10%.

The alkyl chain attached to the rhodanine EG plays a significant role, as it can not only enhance the solubility but also change molecular orientation and affect molecular aggregation. However, complicated and low-yield alkylation of rhodanine termini impede further trials of modification on alkyl group of rhodanine EGs.[67] Recent work demonstrated the effectiveness of esterification on rhodanine EGs in improving photovoltaic performance. Our group designed a pair of BDT-based small molecule donors (i.e. BDT-RO and BDT-RN), which incorporate 2-ethylhexyl and n-octyl esterified rhodanine end groups, respectively. Devices based on BDT-RN: IDIC exhibited severe trap-assisted recombination, whereas BDT-RO: IDIC devices profit from low bimolecular and trap-assisted recombination losses. Consequently, BDT-RO achieved a higher PCE of 9.01% than its isomer BDT-RN (8.36%), which is an 18% enhancement relative to its non-esterified counterpart DR3TBDTT (7.61%).[67] Although tremendous success has been achieved via rational modifying the rhodanine EGs, it not always perform better results in some cases. Our group further synthesized BTR-OH by introducing hydroxyl in the BTR rhodanine EG. Hydroxylation reduces the crystallinity and phase segregation of BTR-OH: $PC_{71}BM$, resulting in the inferior performance of BTR-OH (8.00%) to BTR (9.05%). However, BTR-OH became an excellent third component to the BTR: $PC_{71}BM$ host binary system. The ternary system based on BTR: BTR-OH: $PC_{71}BM$ obtained a champion PCE of 10.14% with BHJ active layer thickness of ≈ 300 nm when 20% BTR is replaced by BTR-OH. BTR-OH is versatile in the ternary system. BTR-OH improved the film absorption, reduced bimolecular/ trap-assisted recombination, suppressed the crystallinity of the donor phase, and fine-tuned the phase-separated network and domain size to a reasonable level.[77]

Several terminal groups other than rhodanine-based terminus are also proven effective in propelling the PCE of BDT-based donors. Li group demonstrated two small molecule donors

(SM1 and SM2) based on the 2D BDT central building block, terthiophene π-bridge, and ester electron-withdrawing EGs with and without cyano substituent (**Figure 4**). SM1 presents stronger absorption, deeper HOMO level, and higher hole mobility, enabling SM1: IDIC-based ASM OSC with a higher PCE of 10.11% in comparison with SM2: IDIC-based counterpart of 5.32% efficiency (**Table 1**). [64] In some cases, such a cyano substituted ester end group exhibits better photovoltaic performance. Li and co-workers reported two medium bandgap alkylsily-thienyl BDT donors, H21 and H22, with 3-ethyl rhodamine and cyanoacetic acid esters as end groups, respectively.[69] (**Figure 4**) The alteration from 3-ethyl rhodamine to cyanoacetic acid esters blue-shifted absorption, slightly downshifted LUMO and upshifted HOMO and enhanced hole mobility. H22: IDIC blend also exhibited a better 3D charge transport channel and a more appropriate crystal size. Therefore, H22 displayed a higher PCE of 10.29% than H11 (7.62%) (**Table 1**).[69]

3.3 Effect of the Side Chain

The side chain engineering is widely employed in the BDT-based small donors to tailor solubility, hole mobility, crystallinity, and BHJ active layer morphology. In some cases, even subtle modifications in the side chains can trigger a significant impact on the photovoltaic performance of ASM OSCs.

The substitution of alkoxyls by alkylthienyls in both 4- and 8- positions of BDT unit has proven to be a feasible and widely used approach to synchronously transfer from one-dimensional (1D) to 2D conjugated structure and enhance planarity of the BDT-based small molecule donors. For instance, Hou group reported two BDT-based small molecule donors named DRTB-O and DRTB-T with identical conjugated backbones but diverse substituted side chains.[61] (**Figure 5**) DRTB-O with alkoxyls formed more ordered aggregation structure than DRTB-T with alkylthienyls, although they possess very similar absorption spectra and molecular energy levels. With $PC_{71}BM$ as acceptor, DRTB-T exhibits a higher PCE of 7.08% than DRTB-O (4.91%). (**Table 1**) Along with IDIC, the DRTB-T presents a significantly higher PCE of 9.06% than DRTB-O (0.15%).[61] Li group also reported H11 and H12 (**Figure 5**), two small molecule donors with 2D BDT and 1D BDT cores, respectively. The 2D-conjugated small molecule H11 presents stronger absorption, lower-lying HOMO energy level, higher hole mobility, and more ordered bimodal crystallite packing than H12 with alkoxyls. Moreover, according to the Hansen

solubility parameters and differential scanning calorimetry measurements, the interaction parameter (χ) was 3.78 in H11: IDIC and 3.52 in H12: IDIC blend film. It indicates a higher phase purity of H11: IDIC blend. These distinctive properties lead to a PCE of 9.73% for H11: IDIC relative to 5.51% for H12: IDIC.[56] Li group further replaced the alkylthienyl in H11 with alkylthio-thienylenevinylene thiophene (TVT-SR) and obtained a new small molecule donor BDT(TVT-SR)$_2$, which enabled broader absorption profile, deeper HOMO energy level and pronounced hole mobility.[70] These factors boosted the PCE of BDT(TVT-SR)$_2$:IDIC-based ASM OSC to 11.10%. (**Table 1**) Besides, BDT(TVT-SR)$_2$ demonstrated better thermal and photostability than H11. Chen and co-workers demonstrated a small molecule donor DR3TSBDT with dialkylthiol-substituted BDT as the electron-donating core.[40] (**Figure 5**) Relative to DR3TBDT with dialkyloxy chains, DR3SBDT with dialkylthiols displayed improved hole mobility, enhanced blend film absorption with $PC_{71}BM$, and a preferable morphology with a domain size of ~15 nm and bicontinuous phase-separated network, which boosted the photovoltaic performance from 7.38% to 9.95% (**Table 1**).[40]

Recently, some research groups have achieved over 13% efficiency of ASM OSCs with halogenated BDT-based small molecule donors. Ge group introduced fluorine atoms to alkylthienyl side chains of BDT-based small molecule donor DCAO3TBDTT and obtained mono-fluorinated BTEC-1F and di-fluorinated BTEC-2F.[79] (**Figure 5**) The BTEC-1F: Y6 exhibited a higher PCE of 11.33% than DCAO3TBDTT: Y6 (10.64%), and the device based on BTEC-2F exhibited a high PCE of 13.34% with a high FF of 72.35%. The PCE enhancement of BTEC-2F: Y6 system is mainly ascribed to the improved phase separation, tighter molecular stacking, and highly ordered face-on orientation in BHJ active layer, which facilitates charge transport and weakens bimolecular recombination.[79] (**Table 1**)

Our group reported a novel small-molecule donor, namely BTR-Cl (**Figure 5**), by introducing a chlorine atom into the side chains of BTR. In comparison to the BTR counterpart, BTR-Cl exhibits a much easier synthesize process and deeper HOMO energy level, resulting in a slightly improved V_{OC} of 0.86*V* when paired with star NFA Y6. In addition, BTR-Cl displays a different liquid crystalline pattern (edge-on) and higher phase transition temperature compared to the nonchlorinated BTR. Eventually, ASM OSC based on BTR-Cl: Y6 exhibited more balanced carrier mobilities, and thus a higher PCE of 13.6% (**Table 1**).[76]

A breakthrough of over 15% efficiency ASM OSCs has been demonstrated very recently. Hou and co-workers designed a 2D conjugated small molecule donor (B1) with phenyl-substituted BDT central building block, which has a larger rotational barrier, increased crystallinity, and remarkably improved PCE than BTR with thiophene-substitution (**Figure 5**). The device based on B1: BO-4Cl delivers an excellent PCE of 15.3% (certified PCE 15.1%), a record-high PCE value for ASM OSCs so far. In contrast, the BTR: BO-4Cl system only obtains 11.3% efficiency.[43] (**Table 1**)

3.4 Effect of π Bridge

The π bridges in BDT-based small molecule donors can be utilized to tune the optical and electrical properties as well as morphological factors. Our group designed two structural isomers, BIHTR and BOHTR, which differ in the hexyl chain positions in the thieno [3,2-b] thiophene and thiophene bridges. BIHTR with inward hexyls has a planar conformation and significantly improved molecular stacking. BIHTR: Y6 has a better morphology than BOHTR: Y6 counterpart. Eventually, ASM OSCs based on BIHTR: Y6 demonstrate improved photovoltaic performance (12.3%) than BOHTR: Y6 (10.8%).[80] (**Figure 6, Table 1**)

Owing to the largely π-extended ring with high electron affinity, copolymer donor with naphtho [1,2-c:5,6-c'] bis [1,2,5]thiadiazole (NT) demonstrated low-lying HOMO and narrow *E*g, strong crystallinities as well as hole mobilities of up to 0.5 $cm^2 V S^{-1}$. It enables polymer solar cells (PSCs) with high performance and good tolerance of active layer thickness. Peng and co-workers first introduced the NT unit as the internal second acceptor block to the small molecule donor and designed BDTTNTTR and BDTSTNTTR (**Figure 6**). As expected, both donors exhibited wide absorption profiles (up to 800 nm), highly planar structures, low-lying HOMO levels (~ -5.3 eV), as well as high hole mobilities (10^{-3} $cm^2 V S^{-1}$). When a halogen-free solvent (carbon disulfide) was used, BDTSTNTTR with sulfur atoms in the side chains demonstrated an excellent PCE of 11.53% with a small E_{loss} of 0.57 eV, outcompeting the BDTTNTTR counterpart (10.02%).[54]

Recently, Ge and co-workers reported BT-2F by changing the positions and the length of alkyls on terthiophene π bridges of BTEC-2F (**Figure 6**). BT-2F with shortened alkyl chains and enhanced regularity displays more ordered molecular arrangement and more compact lamellar stacking. Hence, BT-2F exhibited improved hole mobility, enhanced hole carrier extraction, and

an optimized phase-separated morphology when blended with Y6 or N3. As a result, BT-2F: Y6 and BT-2F: N3 both presented excellent PCEs of 13.80% and 14.09%, higher than BTEC-2F: Y6 (13.34%). [86] (**Table 1**)

To conclude, the design of small molecule donors is of vital importance for the advance of ASM OSCs, since almost every breakthrough advent with wise modification on molecule structures. Be more specific, small molecule materials possess well-defined structures, providing chemists with a clear vision for precisely tailoring the molecule structure towards enhanced photovoltaic performance. Strategies of the core, EG, side chain, and π bridge engineering are discussed in this section to unveil the structure-performance relationship of small molecule donors. For instance, side chain engineering of introducing alkylthienyls in the 4- and 8- positions of BDT unit can transfer from 1D to 2D conjugated structure and boost the PCEs based on BDT small molecule donors. Then, the PCE record values were continually renewed by modified 2D BDT small molecule donors paired with strong NIR-absorbing NFAs (usually Y6 or its derivatives), such as BTR-Cl (13.61%), BSFTR (13.69%) and BT-2F (14.09%). The success of 2D BDT small molecule donors are mainly due to the improved planarity and thus the increased π-π stacking, pronounced crystallinity, deeper HOMO level, and enhanced mobilities. The next PCE growth point may advent base on the novel 2D BDT structure design since the rigid and planar backbone is a key factor to obtain improved photovoltaic performance. The recent breakthrough of phenyl-substituted 2D BDT-based small molecule donor (B1) with 15.3% efficiency demonstrates the strong potential of 2D BDT materials for top-performing ASM OSCs.

4. Device Consideration

Apart from the evolution of small-molecule donors, the realization of excellent PCE also needs donor: acceptor matching, film morphology optimization, and the understanding of photophysics. [1, 2, 4, 6, 39] Below, we discuss several device-relevant aspects of BDT-based small molecule donors.

4.1 Donor-acceptor Matching

The tunable optoelectronic properties of BDT-based small molecule donors widen the selection window of acceptors from which efficient ASM OSCs can be constructed. In general, acceptors need to possess energy levels (such as HOMO, LUMO, and E_{op}) that are sufficient for

engendering efficient charge separation, but can also minimize E_{loss}. The chosen acceptors should absorb sunlight with complementary wavelengths to those absorbed by the donors to maximize light harvesting and therefore the $J_{SC.}$ The acceptors should possess comparable electron mobilities with the hole mobilities of donors, to facilitate charge transport. The donor: acceptor blend exhibited suitable phase separation and molecular orientation to insure efficient charge separation as well as charge percolation routes. [1, 15, 39] IDIC emerged as the pioneer NFA that prompts the photovoltaic performance of ASM OSCs based on NFAs to outperform their fullerene counterparts. It is on account of the pronounced and complementary absorption profile (500 ~ 800 nm in the solid film), which matches BDT-based wide/medium bandgap small molecule donors to potentially obtain high J_{SC}. The high electron mobility of IDIC (up to 10^{-3} $cm^2 V^{-1} s^{-1}$ estimated from SCLC) is advantageous for achieving high FF. Crystallinity and phase aggregation of IDIC based blend can be finely manipulated by thermal annealing (TA) and/or solvent vapor annealing (SVA) posttreatment techniques.[31, 45]

Some optoelectronic properties, such as energy level, can be rationally selected and controlled. Other properties, such as those involving BHJ blend film morphology, are more difficult to predict. Furthermore, many properties are interrelated; for instance, charge mobility has a strong relationship with the morphology. Thus, the choice of the acceptor is sometimes based on trial and error. For instance, the BDT-based small molecule donor BSFTR yields PCEs varying from 6.43% to 13.69% (**Table 1**) when paired with different NFAs – IDIC, Y6, NBDTP-$F_{out,}$ and NBDTP-M_{out}. Despite the difficulty of predicting the morphology, some device parameters can be rationally forecast, such as V_{OC} values. The variance of V_{OC} in BSFTR-based ASM OSCs (from 0.56 to 0.98 V) correlates well with the LUMOs of the chosen acceptors (from -3.94 to -4.10 eV).[83, 84]

4.2 Morphology Control

The morphology of the BHJ active layer is critical to determine the photovoltaic performance of OSC. Generally, to ensure the optimal solar cell operation, the film morphology must satisfy strict requirements. The donor and/or acceptor domain size should be confined to approximately 30 nm to ensure efficient exciton diffusion to D/A interface for the following exciton dissociation. Besides, D/A stacking at the interface area influences exciton dissociation. [26, 32, 49, 66, 91-93] Suitable crystallinity, close π - π stacking, and high domain purity of the donor

and acceptor phases are needed for achieving efficient charge transport. Apart from material design, devices are optimized to realize the above considerations, such as posttreatment and solvent additive strategy.

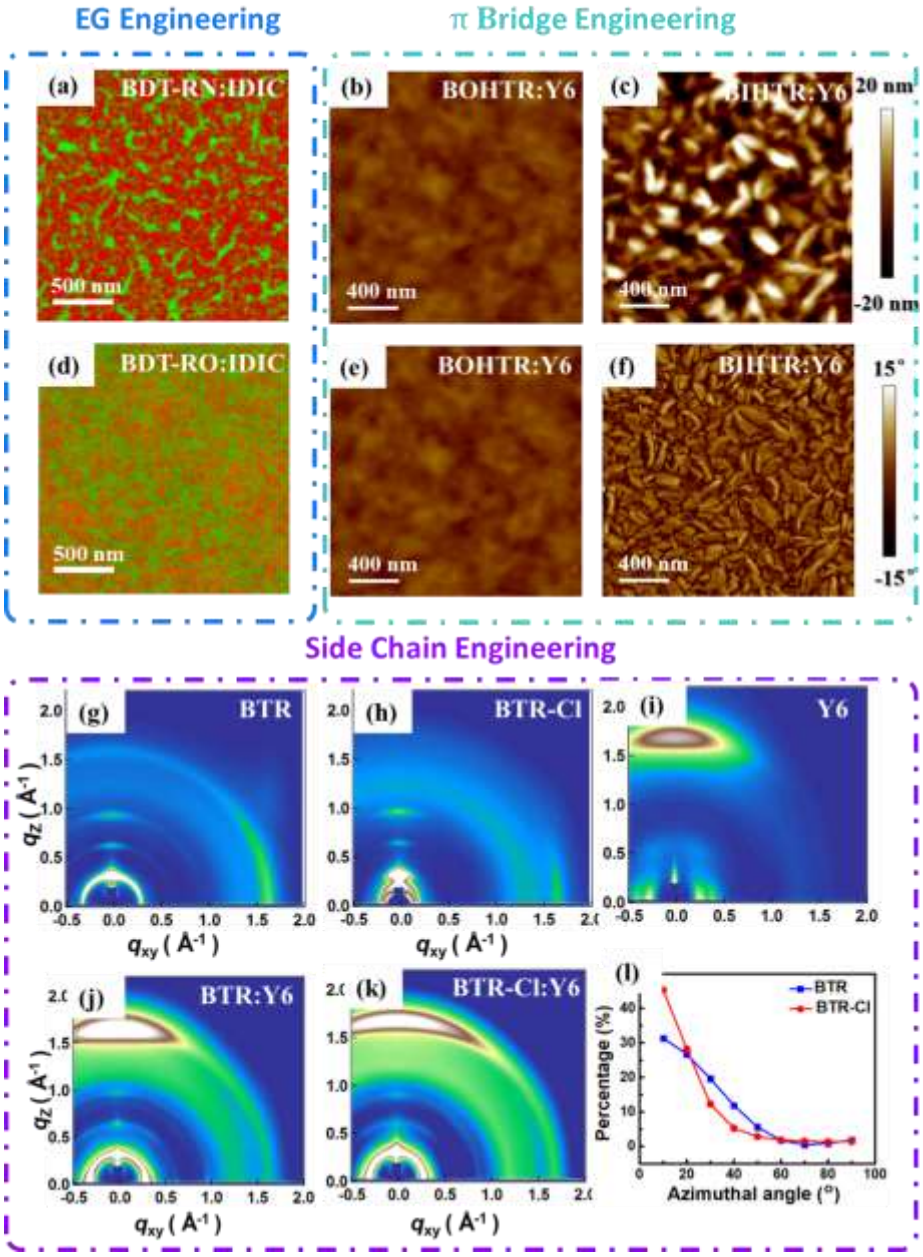

Figure 8. EELS images of BHJ active layers based on (a) BDT-RN: IDIC and (d) BDT-RO: IDIC. (Red: donor-rich domains; green: acceptor-rich domains) Reproduced with permission.[67] Copyright 2019 Royal Society of Chemistry. AFM height images (b) and (c), and phase images (e) and (f) of BOHTR: Y6 and BIHTR: Y6. Reproduced with permission.[80] Copyright 2020, Wiley-VCH. Grazing-incidence wide-angle X-ray scattering (GIWAX) patterns of neat films of

(g) BTR, (h) BTR-Cl, and (i) Y6 and blend films of (j) BTR: Y6 and (k) BTR-Cl: Y6. (l) The intensity azimuthal pole figure of (010) diffractions of BTR and BTR-Cl pure films. Reproduced with permission.[76] Copyright 2019, Elsevier.

4.2.1 Structure Modification

Although we have discussed the chemical structure-property relationship of BDT small molecule donors, we try to convey to readers more specific information about how the structure modification strongly influences the morphology in this paragraph.

The first example is about EG engineering. As aforementioned, our group demonstrated two BDT based small molecule donors, namely BDT-RO and BDT-RN, which only differ in the side chain of the rhodamine group. BDT-RO and BDT-RN exhibit the third-order peak in the OOP direction, and (010) π-π peak in the IP direction, indicating these materials have preferentially edge-on orientation. The CCL of (100) lamellar peak in the pristine BDT-RO is larger than that of BDT-RN, indicative of the better structural order in BDT-RO. High-resolution TEM imaging combined with electron energy loss spectroscopy (EELS) analysis provides the donor-acceptor distribution of the active layers. BDT-RO BHJ active layers exhibited finer scale domains of donor-rich and acceptor-rich phases than their counterparts comprising BDT-RN (**Figure 8a and d)**. Besides, BDT-RO:IDIC ($\mu_h = 3.24 \times 10^{-4}$ cm^2 V^{-1} S^{-1} and $\mu_e = 6.45 \times 10^{-4}$ cm^2 V^{-1} S^{-1}) exhibited higher and more balanced hole and electron mobilities than BDT-RN:IDIC ($\mu_h = 1.87 \times 10^{-4}$ cm^2 V^{-1} S^{-1} and $\mu_e = 5.44 \times 10^{-4}$ cm^2 V^{-1} S^{-1}). Consequently, BDT-RO with 2-ethylhexyl exhibited higher PCE of 9.01% than BDT-RH with n-octyl (8.36%).

π bridge engineering afforded two structural isomers, BIHTR and BOHTR, with different positions of hexyls. From DFT calculations, BIHTR with inward hexyls has a much flatter conformation than BOHTR, which causes differences in intermolecular packing. As AFM height and phase images show (**Figure 8b-c and 8e-f**), BIHTR has stronger aggregation and shapes apparent phase separation with Y6, which is in accordance with the clear petaloid patterns observed from high-angle annular dark-field scanning transmission electron microscopy (HAAD-STEM). According to GIWAXS, BIHTR demonstrated a stronger π–π stacking peak at q_z of 1.76 Å^{-1}(d =3.57 Å) than BOHTR (q_z of 1.71 Å^{-1}), indicating the inward BIHTR possesses a closer face-on π-π stacking and smaller interplanar spacing. This trend is also retained in the

BHJ blend film. Consequently, BIHTR: Y6 presents improved PCE of 12.3% with higher FF of 68.4% and weaker recombination.[80]

In addition to the EG and π bridge engineering, side-chain engineering can also significantly influence the film morphology. By comparing BTR and its chlorinated derivative, BTR-Cl, it is found that Cl in the BDT core can change the orientation distribution of crystallites. Up to 45% of the π-π stacking signal of the BTR-Cl crystallites presented at an azimuthal angle of approximately 10°, indicating a variety of BTR-Cl molecules have a favorable edge-on orientation. (**Figure 8h and l**) On the contrary, only 30% of BTR crystallites displayed the same signal at this azimuthal angle. Nearly 90% of BTR-Cl crystallites displayed a π-π stacking signal with a narrow azimuthal angle scope from 0° to 30°, while 90% of BTR crystallites have a relatively wider azimuthal angle from 0° to 50°. (**Figure 8g-h and l**) Besides, the neat film of BTR-Cl exhibits a closer π-π stacking d-spacing and a larger CCL than the BTR counterpart. Thus, the BTR-Cl molecules are capable of retaining a better edge-on orientation relative to the PEDOT: PSS substrate. As for blend films, BTR-Cl: Y6 BHJ blend film demonstrates an enhanced π-π stacking CCL (010) of 5.23 versus 4.7 nm (BTR: Y6) in IP direction and 4.60 versus. 4.11 nm (BTR: Y6) in OOP directions. The morphology changes enhance PCE from 10.67% (BTR: Y6) to 13.61% (BTR-Cl: Y6).[76] (**Table 1, Figure 8g-i and 8j-l**)

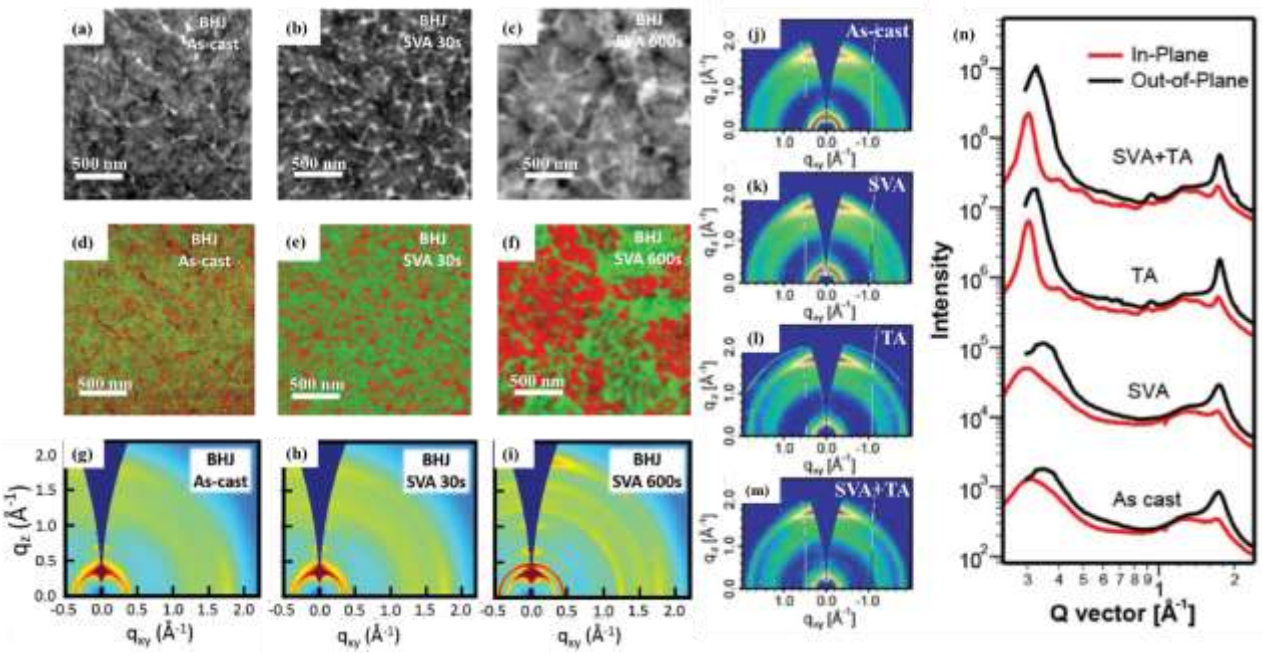

Figure 9. Morphology analyses for DR3TBDTT: O-IDTBR BHJ active layers subjected to various SVA duration: Dark-field scanning transmission electron microscopy (STEM) images of the BHJ active layers of (a) as-cast, (b) SVA 30 s (optimal condition) and (c) SVA 600 s. The corresponding EELS images of (d) as-cast, (e) SVA 30 s, and (f) SVA 600 s. (green: donor-rich domains; red: acceptor-rich domains) The corresponding GIWAXS patterns of (g) as-cast, (h) SVA 30 s, and (i) SVA 600 s. Reproduced with permission.[66] Copyright 2018, Wiley-VCH. The GIWAXS patterns of BSFTR: Y6 BHJ active layers subjected to various conditions of (j) as-cast, (k) SVA, (l) TA, and (m) combination of TA and SVA. (n) The corresponding GIWAXS intensity patterns. Reproduced with permission.[83] Copyright 2019, Wiley-VCH.

Table 2. Summary of photovoltaic performance of top-performing BDT donor-based ASM OSCs with optimal morphology control techniques.

Donor	Acceptor	TA [Temperature/duration]	SVA [Solvent/duration]	Additives	PCE [%] As-cast	PCE [%] Optimized	Ref
SM1	IDIC	115 °C/10 min			5.45	10.11	[64]
SM2	IDIC	110 °C/10 min			0.86	5.32	[64]
BIHTR	Y6	115 °C/10 min			0.5	12.3	[80]
BOHTR	Y6	115 °C/10 min			2.1	10.8	[80]
H11	IDIC	120 °C/10 min			5.37	9.73	[56]

H12	IDIC	120 ℃/10 min		1.83	5.51	[56]
BDT(TVT-SR)$_2$	IDIC	110 ℃/10 min		5.69	11.10	[70]
H21	IDIC	130 ℃/5 min		/	7.62	[69]
H22	IDIC	130 ℃/5 min		/	10.29	[69]
DCAO3TBDTT	Y6	130 ℃/10 min	0.4% CN	0.54	10.64	[79]
BTEC-1F	Y6	130 ℃/10 min		1.05	11.33	[79]
BTEC-2F	Y6	130 ℃/10 min	0.4% CN	6.69	13.34	[79]
BT-2F	Y6	130 ℃/10 min		8.94	13.80	[86]
	N3	100 ℃/10 min		/	14.09	[86]
BDTT-TR	Y6	140 ℃/2 min		0.12	12.18	[94]
BTR	$PC_{71}BM$		THF/15 s	5.2	9.3	[41]
	Y6	100℃/10min		/	10.67	[76]
	BO-4Cl		CB/40 s	/	10.4	[43]
	BO-4Cl		CF/40 s	/	11.3	[43]
BTR-Cl	Y6	120 ℃/10 min		/	13.61	[76]
B1	BO-4Cl		CB/50 s	/	15.3	[43]
	BO-4Cl		CF/60 s	/	15.0	[43]
DR3TBDTT	O-IDTBR		DMDS/30 s	3.4	6.4	[66]
	IDIC		DMDS/60 s	2.5	8.7	[26]
DRBDT-TT	$PC_{71}BM$		CF/90 s	6.85	8.70	[75]
DRBDT-STT	$PC_{71}BM$		CF/120 s	5.57	8.01	[75]
BDT-RO	IDIC		CS_2/20 s	3.82	9.01	[67]
BDT-RN	IDIC		CS_2/20 s	/	8.36	[67]
SBDT-BDD	$PC_{71}BM$		CS_2/45 s	4.7	8.1	[88]
	IDIC		CS_2/45 s	4.8	9.2	[88]
DR3TSBDT	$PC_{71}BM$	100 ℃/10 min	CF/60 s	6.62	9.95	[40]
BDT3TR-SF	NBDTP-F_{out}	80 ℃/NA	THF/60 s	6.08	11.02	[81]
	NBDTP-M	100 ℃/5 min	THF/90 s	4.18	10.23	[82]

BSFTR	Y6	120 ℃/5 min	CF/40 s		0.22	13.69	[83]
2F-C_4C_6	IDIC			0.4% CP	5.17	6.21	[90]
2F-C_6C_8	IDIC			0.4% CP	6.42	8.23	[90]
BDTT-S-TR	NIDCS-MO			0.75% DIO	1.09	4.67	[74]
				3% DTBT		2.31	[74]
				0.75% DIO + 2% DTBT		5.33	[74]
SMPV1	$PC_{71}BM$			0.5 mg ml^{-1} PDMS	7.2	8.1	[68]
O-BDTdFBT	$PC_{71}BM$			0.5% DIH	6.02	8.10	[95]
DR3TBDTT	IDTTBM			0.8% DIO	0.8	4.4	[50]
SMPV1	IDTTBM			0.8% DIO	0.7	4.4	[50]
BTR	IDTTBM			0.5% DIO	0.4	2.4	[50]
BTR-Cl	Y6	120 ℃/10 min		0.3% DIO	/	14.7	[29]

THF: tetrahydrofuran; CB: chlorobenzene; CF: chloroform; DMDS: dimethyl disulfide; CS_2: carbon disulfide; CN: 1-chloronaphthalene; CP: 2-chlorophenol; DIO: 1,8-diiodooctane; DTBT: di-2-thienyl-2,1,3-benzothiadiazole; PDMS: polydimethylsiloxane; DIH: diiodohexane.

4.2.2 Posttreatment Techniques

Many top-performing solution-processed ASM BHJs have achieved excellent PCEs by optimizing active-layer morphology via alteration of device processing parameters, which include blend ratios, film thicknesses, temperatures, and durations for TA, solvents, and durations for SVA, and additive concentrations. Among which TA, SVA, and the combination of TA and SVA are proven to be the most efficient posttreatment techniques in top-performing ASM OSCs. **Table 2** summarizes the best-performing BDT donor-based ASM OSCs utilizing approaches to optimize the morphology.

TA is a widely employed morphology optimization procedure, which is usually carried out by heating the as-cast BHJ active layer on a hot plate with a temperature usually ranging from 70 °C to 200 °C for several minutes. TA generally enhanced crystallinity, phase aggregation, and phase separation through the improved molecular kinetic motion in the BHJ films induced by heating. Specific procedures vary in different ASM systems, but the dominant TA conditions do not deviate far from 100 °C for 10 minutes. **Table 2** summarizes the high-performance ASM

OSCs with optimal morphology control techniques. Among them, TA often improves the performance of the ASM OSCs and turns into a common device optimization protocol.[39] Many high-performing ASM systems based on BDT-based small molecule donors obtain the optimized PCEs after TA treatment [64, 80, 56, 70, 69. 76, 79, 83, 86, 96] For instance, Min group demonstrated that TA significantly improves the PCE of BDTT-TR: Y6 system from 0.12% to 12.18%. They first carry out UV-Vis absorption spectroscopy to check the influence of TA treatment on film properties. In contrast to the as-cast blend films, the annealed blend films display a red-shifted absorption profile with distinct peaks at approximately 600 nm, showing improved aggregation of photoactive materials. As shown in TEM images, the BDTT-TR: Y6 as-cast film almost exhibited no discernible structure, implying a finely intermixed D/A microstructure without obvious crystallization or phase separation. In contrast, BDTT-TR: Y6 annealed film presented clear D/A domains with a bi-continuous interpenetrating network. GIWAXS demonstrated that the as-cast BDTT-TR: Y6 film only exhibited scattering rings with π-π stacking peak at 1.70 $Å^{-1}$, while the annealed film exhibited strong third-order lamellar peaks and strong bimodal π-π peak. The increased crystallinity and strengthened D/A phase separation account for dramatic increased PCE from 0.12% to 12.18% and FF from 22.25% to 66.06%.[94]

SVA is typically performed by exposing the as-cast BHJ active layer to solvent vapor in a relatively sealed environment for a duration of several seconds to several minutes. The solvent vapor is capable of permeating into the active layers which provides an atmosphere for the molecular movement of donor and/or acceptor in the BHJ films. The SVA procedures for the best results usually vary significantly in different ASM systems. It is because of factors including the respective solubilities of the donor and/or the acceptor in the solvent vapor, the partial vapor pressure of the solvent on the BHJ films, as well as the exposure duration. Although the research communities have no clear agreement on details such as whether a good solvent for both donor and acceptor or only for one of them is preferential for optimizing the BHJ film morphology and the impact on the device stability, SVA remains a universal approach to fine-tune the ASM blend films towards enhanced PCEs.[32, 41, 50, 66]

We utilized the THF SVA process to significantly improve PCE of BTR: $PC_{71}BM$ based ASM OSCs from 5.2% to 9.3%.[41] According to dark *J-V* curves, the SVA treated device demonstrated notably enhanced current density under positive bias relative to the as-cast counterpart. In contrast, the current density was one order of magnitude smaller in reverse bias.

SVA treatment reduces series resistance (R_s) by six times and slightly increases shunt resistance (R_{sh}). SVA strategy is capable of suppressing the leakage current and enhancing the diode behavior, which is mainly attributed to the morphology evolvement through THF SVA. As-cast BTR: $PC_{71}BM$ blend presents fine crystal domains and random pinholes, which are presumably attributed to the escape of processing solvent. After a 15 s THF SVA treatment, the BHJ active layer presents a coarser surface, and the pinholes disappear. Both the TEM tomograms and the corresponding computer models have shown that small domains in the as-cast BHJ blend film evolve into larger domains which interpenetrated to construct 3D charge highways throughout the entire BHJ blend film after THF annealing, and thus benefit charge transport. As shown in GIWAXS data, SVA increases the crystallinity and reduced the π-π stacking distance of surface BTR ordering (from 3.80 to 3.60 Å). The random orientation of the BHJ active layer evolves into the co-existence of both face-on and edge-on molecule orientation after the SVA procedure.

Beaujuge and co-workers demonstrated that the PCE of DR3TBDTT: O-IDTBR was doubled to 6.4% from the initial 3.4% via 30 s dimethyl disulfide (DMDS), which is then reduced to 1.1% under prolonged SVA. They systematically characterized the benefits and limitations of the SVA treatment subject. As donors and NFAs typically do not provide sufficient contrast in images from standard TEM, EELS and STEM are combined to study morphology. The as-cast film presents small-sized (up ~ 50 nm) s donor- and acceptor-rich domains and film with SVA 30 s display larger D: A network (up ~ 70 nm). When exposed to solvent vapor for 600 s, the active layer presents excessively large size (up ~ 800 nm) of small molecule donor and acceptors, which may hinder exciton migration to interfacial zones and exciton dissociation into charge carrier.[66] (**Figure 9 a-f**) GIWAXS data for blend films were collected. (**Figure 9 g-i**) The blend film scattering profile possesses an overlap of scattering from the pure DR3TBDTT and O-IDTBR, indicating that the donor and acceptor in the BHJ film do not construct a finely mixed structure. When subjected to SVA for 30 s, only tiny variations to the integrated scattering are demonstrated. After SVA for 600 s, O-IDTBR presents a new crystal structure, and its alkyl and π–π stack peaks become anisotropic, implying a lack of uniform molecular orientation. According to other characterization techniques including transient photovoltage (TPV), transient photocurrent (TPC), light-intensity-dependence, and time-delayed collection field (TDCF), the optimized morphology via 30 s SVA reduce the nongeminate and the geminate recombination thereby enhances the PCE.

TA and SVA posttreatment techniques are sometimes combined to modulate morphology. Chen and co-workers designed a new small molecule donor material DR3TSBDT and achieved a PCE of 6.62% along with $PC_{71}BM$, which was improved to 9.95% via the combination of TA and SVA. As shown in TEM images, better phase separation could be observed after the TA processing than that of the as-cast film. With further SVA treatment, clear nanoscale phase separation with the domain size of approximately 15 nm and a bi-continuous interpenetrating network was observed in BHJ active layer, which served for exciton dissociation and charge transport. As seen from GIWAXS, the scattering of (h00) and (010) was both intensified for neat and blend films with TA and SVA treatment, which indicates a more ordered structure after two-step treatments and promote charge transport. A similar case can also be found in over 13% efficiency BDT-based ASM OSCs. As shown in **Figure 9 j-n**, Zhu and co-workers sequentially optimize the BSFTR: Y6 BHJ active layers by SVA, TA, and SVA&TA. They found out that SVA can slightly promote the molecular crystallinity, but TA can dramatically enhance the crystallinity with an extra peak. When combining both posttreatment techniques together, blend film exhibited slightly decreased crystallinity with more ordered donor and acceptor phase in comparison to only TA treatment, which leads to the high efficiency of 13.69%.[83] (**Table 2**)

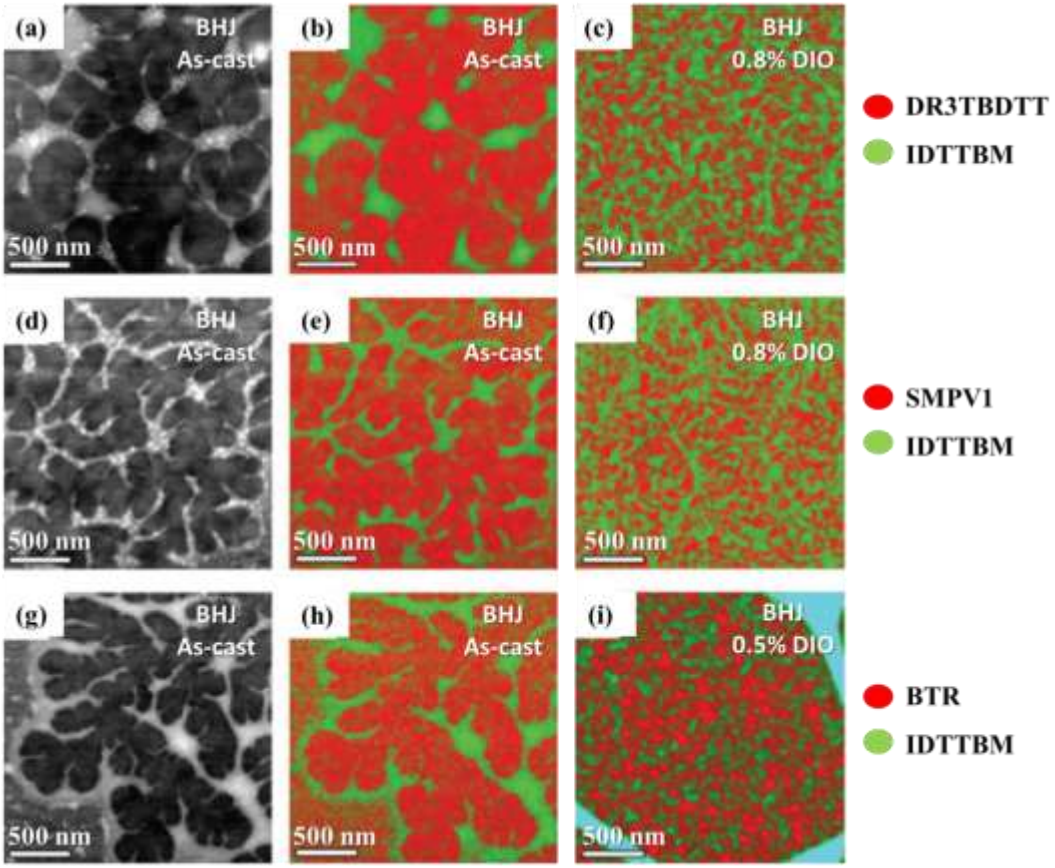

Figure 10. BHJ active layers of DR3TBDTT: IDTTBM: STEM image of (a) as-cast, EELS images of (b) as-cast, and (c) optimized with 0.8% DIO. BHJ active layers of SMPV1: IDTTBM: STEM image of (d) as-cast, EELS images of (e) as-cast, and (f) optimized with 0.8% DIO. BHJ active layers of BTR: IDTTBM: STEM image of (g) as-cast, EELS images of (h) as-cast, and (i) optimized with 0.5% DIO. (green: donor-rich domains; red: acceptor-rich domains) Reproduced with permission.[50] Copyright 2018, Wiley-VCH.

4.2.3 Solvent Additive Strategy

Adding a tiny amount of solvent additive in the prepared BHJ solution is a simple and effective method to alter the kinetics to facilitate the molecular reconstruction of the donor and/or acceptor materials during the BHJ film formation. The solvent additive usually possesses a higher boiling point and different solubility for donor and/or acceptor compared to the host solvent. Frequently-used solvent additives include 1,8-diiodooctane (DIO), 1-chloronaphthalene (CN), and 2-chlorophenol (CP).[1, 31, 39] Also, the amount of solvent additive is generally no more than 1% in volume respect to the host solvent in ASM systems, since the ASM-based BHJ films are

extremely sensitive to device optimization procedures. Beaujuge and co-workers employed three ASM systems (DR3TBDTT: IDTTBM, SMPV1: IDTTBM, and BTR: IDTTBM) to unveil the impacts of high boiling point solvent additive (DIO) on the BHJ film morphology. The STEM images (**Figure 10 a, d** and **j**) and EELS images (**Figure 10 b, e** and **h**) of as-cast BHJ films of these three systems have shown that all the small molecule donors are very easy to aggregate, which result in the large scale of donor-rich domains ($\approx$ 200 nm). The excessive large domains lead to severe geminate recombination, and thus poor PCEs of 0.8% (DR3TBDTT: IDTTBM), 0.7% (SMPV1: IDTTBM) and 0.4% (BTR: IDTTBM). The introduction of DIO in the processing solution effectively fine-tune the length scale of the donor-acceptor network (**Figure 10 c, f** and **i**), and thus significantly reduces the geminate recombination and improve the carrier mobilities, which yield the enhanced PCEs of 4.4% (DR3TBDTT: IDTTBM), 4.4% (SMPV1: IDTTBM) and 2.4% (BTR: IDTTBM).[50] This work also found that when the DIO content increased to over 1% in the processing solution of DR3TBDTT: IDTTBM, the donor-rich domains have the tendency to grow but the acceptor-rich domains trend to prevail in the BHJ film morphology. High boiling point solvent additive is also utilized in the optimization of O-BDTdFBT: $PC_{71}BM$. Wei and co-workers demonstrated that 1,8-diiodohexane (DIH) is capable of solving the insufficient phase separation issue of BDTdFBT: $PC_{71}BM$ system by inducing the generation of homogeneous grains, which result in the dramatical improvement of FF from 57% to 70%, and slightly enhanced J_{SC} from 10.31% to 11.48%.[95]

In addition to the high boiling point solvent additive, the insulating polymer additive such as PDMS shows its effectiveness in controlling the BHJ film morphology. Yang and co-workers reported that PDMS possesses a similar effect in SMPV1: $PC_{71}BM$ BHJ films with a high boiling point solvent in other ASM systems. The addition of 0.5 mg ml^{-1} PDMS can reduce the average domain size of the SMPV1: $PC_{71}BM$ BHJ film from 50 nm (as-cast control) to 20 ~ 30 nm. PDMS can also lead to more obvious nano-fibrillar phase separation. The suitable domain size and clearer nano-fibrillar phase separation jointly contribute to more efficient exciton diffusion and more effective charge generation and eventually promote the PCE of SMPV1: $PC_{71}BM$ from 7.2% to 8.1%.[68]

In brief, controlling the morphology of ASM OSCs has always been a challenging task, since the BHJ film morphology is easy to change but extremely hard to achieve the optimal condition. Basically, the research community solves the issue via material modification and

device engineering. The chemists need to focus on the structure modification to lead to close π–π stacking and a strong tendency to self-assemble to almost optimal BHJ film morphology. The purpose of device experts is to develop a simple strategy to obtain bicontinuous and interpenetrated donor-acceptor phase separation with domain size of ≈ 20 nm, as well as strong crystallinity.

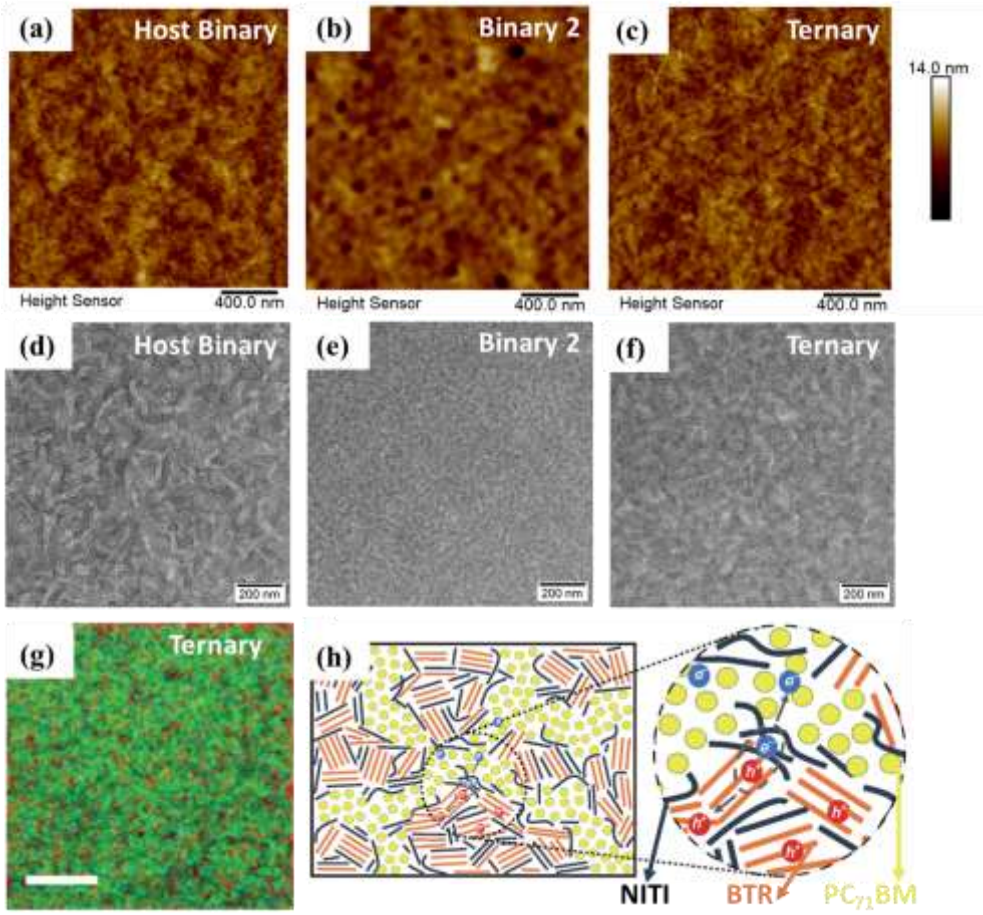

Figure 11. AFM height images (a-c) and TEM images (d-f) of (a, d) BTR:$PC_{71}BM$ host binary, (b, e) BTR-OH:$PC_{71}BM$ binary, and (c, f) BTR:BTR-OH:$PC_{71}BM$ ternary blends. Reproduced with permission.[77] Copyright 2019, Wiley-VCH. (g) EELS image of DR3TBDTT:IDIC:$PC_{71}BM$ ternary blend. (green: donor-rich domains, red: NFA-rich domains and blue: fullerene acceptor-rich domains) Reproduced with permission.[26] Copyright 2019, Wiley-VCH. (h) Illustration of the hierarchical morphology in the BTR:NITI:$PC_{71}BM$ ternary film with dominant charge generation and transport processes. Reproduced with permission.[97] Copyright 2018, Nature Publishing Group.

Table 3. Ternary ASM OSCs with PCEs over 10% based on BDT donors.

The Host Binary ASM OSCs					The Ternary ASM OSCs					
Active layer	V_{OC} [V]	J_{SC} [mA cm^{-2}]	FF [%]	PCE [b] [%]	The third component [D or A]	V_{OC} [V]	J_{SC} [mA cm^{-2}]	FF [%]	PCE [b] [%]	Ref
DCAO3TBDTT: IDIC	0.91	15.53	66.9	9.49	D: DR3TBDTT-S-E	0.91	16.37	67.4	10.04	[98]
BTR: $PC_{71}BM$	0.93	13.95	69.6	9.05	D: BTR-OH	0.93	14.03	74.2	10.14	[77]
BTR: $PC_{71}BM$	0.92	13.40	75.9	9.37	D: FSM6	0.95	13.85	77.6	10.21	[99]
DR3TBDTT: $PC_{71}BM$	0.88	13.52	74.9	8.90	D: DR3TBDTT-E	0.90	14.97	76.5	10.26	[100]
BTR: $PC_{71}BM$	0.90	14.37	72.4	9.37	D: DIB-SQ	0.90	15.44	73.8	10.3	[101]
DR3TBDTT: $PC_{71}BM$	0.90	13.37	74.8	9.09	D: DR3TBDTT-S-E	0.91	14.89	76.9	10.38	[98]
DRTB-T: IDIC	0.99	14.31	62.9	8.90	A: $PC_{71}BM$	0.99	15.47	67.7	10.48	[102]
DR3TBDTT: IDIC	0.87	15.2	64	8.7	A: $PC_{71}BM$	0.87	16.3	72	10.8	[26]
SBDT-BDD: IDIC	0.97	15.15	62.5	9.2	A: $PC_{71}BM$	0.97	16.21	69.3	10.9	[88]
DR3TSBDT: Y6	0.88	21.67	55.21	10.53	A: $PC_{71}BM$	0.86	22.19	67.27	12.84	[103]
BTR: NITI	0.95	15.02	48.69	6.82	A: $PC_{71}BM$	0.94	19.50	73.83	13.63	[97]
BTR-Cl: Y6	0.83	23.79	69.63	13.81	A: $PC_{71}BM$	0.84	23.75	77.11	15.34	[104]

5. Ternary Strategy

A variety of research angles have been contributed to the advance of ASM OSCs. In addition to the aforementioned ones, including material modification and device engineering (such as TA, SVA, and solvent additive strategy), the ternary strategy is another interesting angle as a booming effective method. This strategy via introducing a third component into the donor/acceptor binary materials can broaden absorption, improve exciton dissociation, facilitate charge transport, and fine-tune the BHJ active layer morphology towards enhanced photovoltaic performance.[3, 91, 105-113] Generally, four models have been proposed on the role of the third component in the BHJ active layer of polymer OSCs first - charge transfer, energy transfer, parallel linkage, and alloy models.[3, 114] Also important is the molecular structural compatibility of the multiple components.

For instance, one of us, Li, Yang and coworkers have shown the polymer donors need to be structurally compatible for optimizing morphology in multiple donor polymer solar cells.[106]

ASM OSCs share similarities with PSCs, while at the same time have some distinct features, such as stronger crystallization and aggregation tendency of the former kind. ASM OSCs are usually much more sensitive to the third component incorporation. Thus, the abovementioned models are useful, but cannot well explain the mechanism in ternary ASM OSCs to direct the third component selection.[77, 99] Some high-performing ternary ASM OSCs based on BDT small molecule donors are summarized in **Table 3**. Two main avenues are effective in BDT-based ternary ASM OSCs: (i) introducing a donor compatible in structure but with different crystallinity (easier to tune in small molecules) to fine-tune the morphology of host binary blend; (ii) adding a fullerene acceptor to optimize the morphology and improve charge transport.

The first approach appeals to many research groups. We demonstrated that the donor derivative third component featuring a similar chemical structure but different crystallinity could simultaneously manipulate the crystallinity, domain size, and phase separation of the BHJ active layer morphology to a suitable level.[77] The BTR: $PC_{71}BM$ host binary blend presents more phase-separated D-A networks (**Figure 11d**) with strong crystallinity, which results in relatively weak photovoltaic performance (9.05%). By contrast, BTR-OH: $PC_{71}BM$ binary blend gave an inferior PCE of 8.00% with weaker crystallinity and phase separation (**Figure 11e**). The ternary system exhibits a uniform and smooth film (**Figure 11a-c**) with a suitable crystallinity domain size of ≈ 20 nm, which yield an improved PCE of 10.14% with an active layer thickness of ≈ 300 nm.[77] There are some other examples of incorporating compatible donor derivative as the third component, including BTR: $PC_{71}BM$ (third component: FSM6),[99] DCAO3TBDTT: IDIC (third component: DR3TBDTT-S-E),[98] DR3TBDTT: $PC_{71}BM$ (third component: DR3TBDTT-E)[100] and DR3TBDTT: $PC_{71}BM$ (third component: DR3TBDTT-S-E) systems[98]. (**Table 3**)

Introducing fullerene acceptor third component to the host binary blend is another ternary strategy. Beaujuge and co-workers reported that $PC_{71}BM$ as a third component could be finely dispersed in the DR3TBDTT: IDIC system (**Figure 11g**) to tune the BHJ active layer morphology, which resulted in the dramatically enhanced electron mobility, carrier lifetimes and thus device performance.[26] Zhu and co-workers demonstrated that a hierarchical morphology can be formed by synergizing fullerene and NFAs (**Figure 11h**).[97] It is shown that $PC_{71}BM$ in the BHJ active layer phase separates with the NITI and BTR and construct a hierarchical morphology. In this

scenario, the CT state of BTR: $PC_{71}BM$ can be suppressed to reduce the energy loss, and the charge transport can be enhanced via a cascading energetic channel, thus contribute to the photovoltaic performance improvement.[97] Recently, based on BTR-Cl: Y6 system, our group obtained 15.34% efficiency with $PC_{71}BM$ as the third component and renewed the record value for ASM OSCs. We showed 5 wt% $PC_{71}BM$ incorporation significantly reduce the bimolecular recombination, transform the edge-on orientation to face-on and form microstructures beneficial for charge separation and transportation in the vertical direction, which dramatically boosts the FF from 69.63% to 77.11% and the PCE from 13.81% to 15.34%.[104] (**Table 3**)

6. Conclusion and Future perspectives

ASM OSCs based on BDT small molecule donors have now exceeded 15% in the laboratory generally considered viable for commercialization, on account of the tremendous effort in material design, morphology control, and device physics. However, several challenges still hinder the commercialization of ASM OSCs.

6.1 Material Design Towards Improved PCE

The tiny modification on the chemical structure of small molecule donor and/or acceptor may trigger huge photovoltaic performance differences, and thus the molecule structure-property relationship requires systematic investigation. As for small molecule donors, recent breakthroughs indicate that high-performance BDT-based small molecule donors generally possess a 2D conjugated structure with rhodanine-based EG. The 2D structure effectively improves the planarity which is preferential for charge carrier transport. And the rhodanine EG has been the dominant acceptor moiety choice for efficient BDT-based small molecule donors due to its suitable electronegativity. Thus, the modification (including core, EG, side chain, and π bridge engineering) on the aforementioned 2D conjugated structure may deliver the next record PCE. The success of BTR-Cl (13.61%), BSFTR (13.69%), and B1 (15.3%) possessing such molecule structures have also proven its effectiveness on the enhancement of device performance. As for small molecule acceptor, the emerging NFAs with strong NIR absorption (especially Y6 and its derivatives) can harvest more light with a wide/medium bandgap BDT-based small molecule donor. The advance of NIR NFAs needs the rational design of small molecule donors (especially BDT-based) to meet the donor-acceptor matching criteria (see detail in section 4.1).

Besides, most high-performance NFAs (such as ITIC which is regarded as a star material for PSCs) do not give expected high performance in ASM systems. The mechanism behind the NFA selectivity in ASM OSC is of great interest to the field, which deserves significant investigation in material design, along with device physics and engineering.

6.2 Morphology Control for Scale-up Production

In consideration of the scale-up production, the morphology control techniques need to be as easy as possible. However, the widely used posttreatment techniques, such as TA and SVA, are relatively complicated and incompatible with the scale-up process. For example, we recently reported a simple and effective concentration-induced morphology control method to promote the performance of ASM OSCs based on BDT-based small-molecule donors and fullerene/non-fullerene acceptors (BTR:$PC_{71}BM$ and BTR-Cl:Y6). This approach was found to manipulate the BHJ film morphology by a simply subtle change of the processing solution concentration. Therefore, developing manufacturing friendly morphology control techniques are possible and important for the scale-up production of ASM OSCs.

6.3 Commercialization and Stability Consideration

The potential for commercialization also requires cost-effective material synthesis (including short synthesis route and easy purification process), environmentally friendly processing-more specifically, developing simple and industrial compatible synthesis method with easy purification process, and selecting the green processing solvent and ambient fabrication process. These two areas are rarely explored for ASM systems. So far, some research groups have reported several non-halogenated solvents, such as CS_2 and 2-methyl THF, to replace halogenated solvents such as CF, CB, and o-dichlorobenzene (ODCB), and attempted to fabricate the device in the air. However, some non-halogenated solvents are still toxic and the PCEs of ASM systems via ambient fabrication still lag behind their counterparts fabricated in nitrogen. Also critical is the stability, photo and/or heat-stable donor, acceptor and interfacial materials, steady active layer morphology, as well as effective encapsulation technique, are needed to deliver high-performance and stable ASM OSC products.

6.4 Ternary and Tandem ASM OSCs

The study of ternary ASM OSCs lags far behind the ASM binary systems. The PCEs of the reported best-performing ternary and tandem ASM OSCs are still at a similar level of the binary systems, giving much space to further improve the photovoltaic performance of ASM OSCs. The

bottleneck for the ternary strategy is generally on the third component selection since only two main avenues are reported for ternary OSCs, including (i) introducing a compatible donor with different crystallinity; (ii) adding a fullerene acceptor to optimize the morphology and improve charge transport. Using two NFAs to construct ASM ternary OSCs has rarely been reported, although it is a very effective approach in improving performance polymer OSCs. Besides, tandem solar cells bearing ASM subcells are rarely reported. In view of the better solubility of small molecule donor than polymeric donors, it is difficult to fabricate high-performance solution-processing ASM/ASM based tandem solar cells, as the solution-processing of rear cells influences the vulnerable ASM active layer underneath. In this light, a high-performance tandem device based on ASM rear subcell and PSC front cell seems to be realized more easily.

In summary, we believe ASM OSCs have a bright future. Versatile ASM OSCs in semitransparent and flexible form factors could be employed in many fields, such as solar-generating smart devices (e.g., smartphones, watches, and laptops), the intelligent window for building-integrated photovoltaics, and solar-based automobiles. While more efforts need to be dedicated to innovative products and address the challenges, the opportunities of the next-generation organic photovoltaic technology will continue to improve our lives towards a greener, cleaner, and brighter future.

Acknowledgments

S. Lu thanks the support from research grants from the National Youth Thousand Program Project (R52A199Z11), the National Special Funds for Repairing and Purchasing Scientific Institutions (Y72Z090Q10) and the “Artificial Intelligence” Key Project of Chongqing (No. cstc2017rgzn-zdyfX0030). G. Li and C. Yan thank the support from Research Grants Council of Hong Kong (Project Nos 15218517, C5037-18G), Shenzhen Science and Technology Innovation Commission (Project No. JCYJ20170413154602102), Sir Sze-yuen Chung endowed professorship and the funding for Project of Strategic Importance (Project Code: 1-ZE29), and Postdoctoral Fellowships Scheme (PDFS. Code: YW3Y) provided by the Hong Kong Polytechnic University.

Author Contributions

Conceptualization, C. Y., G. L., and S. L.; Methodology, H.T., C. Y., G. L., and S. L.; Writing – Original Draft, H. T.; Writing – Review & Editing, H. T., C. Y., J. H., G. L., and S. L.; Resources, Z. X., K. S.; Supervision, Z. K., G. L. and S. L.

Reference

1. C. Yan, S. Barlow, Z. Wang, H. Yan, A. K. Y. Jen, S. R. Marder and X. Zhan. (2018). Non-fullerene acceptors for organic solar cells. Nat. Rev. Mater. 3, 18003.
2. G. Li, W.-H. Chang and Y. Yang. (2017). Low-bandgap conjugated polymers enabling solution-processable tandem solar cells. Nat. Rev. Mater. 2, 17043.
3. L. Lu, M. A. Kelly, W. You and L. Yu. (2015). Status and prospects for ternary organic photovoltaics. Nat. Photon. 9, 491-500.
4. P. Cheng, G. Li, X. Zhan and Y. Yang. (2018). Next-generation organic photovoltaics based on non-fullerene acceptors. Nat. Photon. 12, 131-142.
5. D. M. Chapin, C. S. Fuller and G. L. Pearson. (1954). A New Silicon p-n Junction Photocell for Converting Solar Radiation into Electrical Power. J. Appl. Phys. 25, 676-677.
6. G. Li, R. Zhu and Y. Yang. (2012). Polymer solar cells. Nat. Photon. 6, 153-161.
7. J. Zhang, H. S. Tan, X. Guo, A. Facchetti and H. Yan. (2018). Material insights and challenges for non-fullerene organic solar cells based on small molecular acceptors. Nat. Energy 3, 720-731.
8. S.-Y. Chang, P. Cheng, G. Li and Y. Yang. (2018). Transparent Polymer Photovoltaics for Solar Energy Harvesting and Beyond. Joule 2, 1039-1054.
9. G. Zhang, J. Zhao, P. C. Y. Chow, K. Jiang, J. Zhang, Z. Zhu, J. Zhang, F. Huang and H. Yan. (2018). Nonfullerene Acceptor Molecules for Bulk Heterojunction Organic Solar Cells. Chem. Rev. 118, 3447-3507.
10. L. Lu, W. Chen, T. Xu and L. Yu. (2015). High-performance ternary blend polymer solar cells involving both energy transfer and hole relay processes. Nat. Commun. 6, 7327.
11. J. Hou, O. Inganas, R. H. Friend and F. Gao. (2018). Organic solar cells based on non-fullerene acceptors. Nat. Mater. 17, 119-128.
12. Y. Zang, C. Z. Li, C. C. Chueh, S. T. Williams, W. Jiang, Z. H. Wang, J. S. Yu and A. K. Jen. (2014). Integrated molecular, interfacial, and device engineering towards high-performance non-fullerene based organic solar cells. Adv. Mater. 26, 5708-14.
13. Y. Lin, Y. Li and X. Zhan. (2012). Small molecule semiconductors for high-efficiency organic photovoltaics. Chem. Soc. Rev. 41, 4245-72.
14. P. Cheng and X. Zhan. (2016). Stability of organic solar cells: challenges and strategies. Chem. Soc. Rev. 45, 2544-82.
15. H. Yao, L. Ye, H. Zhang, S. Li, S. Zhang and J. Hou. (2016). Molecular Design of Benzodithiophene-Based Organic Photovoltaic Materials. Chem. Rev. 116, 7397-457.
16. L. Lu, T. Zheng, Q. Wu, A. M. Schneider, D. Zhao and L. Yu. (2015). Recent Advances in Bulk Heterojunction Polymer Solar Cells. Chem. Rev. 115, 12666-731.

17. P. Cheng and Y. Yang. (2020). Narrowing the Band Gap: The Key to High-Performance Organic Photovoltaics. Acc. Chem. Res. 53, 1218-1228.
18. J. You, L. Dou, K. Yoshimura, T. Kato, K. Ohya, T. Moriarty, K. Emery, C. C. Chen, J. Gao, G. Li and Y. Yang. (2013). A polymer tandem solar cell with 10.6% power conversion efficiency. Nat. Commun. 4, 1446.
19. I. Mathews, S. N. Kantareddy, T. Buonassisi and I. M. Peters. (2019). Technology and Market Perspective for Indoor Photovoltaic Cells. Joule 3, 1415-1426.
20. H. Spanggaard and F. C. Krebs. (2004). A brief history of the development of organic and polymeric photovoltaics. Sol. Energy Mater. Sol. Cells 83, 125-146.
21. C. W. Tang. (1986). Two-layer organic photovoltaic cell. Appl. Phys. Lett. 48, 183-185.
22. G. Yu, J. Gao, J. C. Hummelen, F. Wudl and A. J. Heeger. (1995). Polymer Photovoltaic Cells: Enhanced Efficiencies via a Network of Internal Donor-Acceptor Heterojunctions. Science 270, 1789-1791.
23. Q. Liu, Y. Jiang, K. Jin, J. Qin, J. Xu, W. Li, J. Xiong, J. Liu, Z. Xiao, K. Sun, S. Yang, X. Zhang and L. Ding. (2020). 18% Efficiency organic solar cells. Science Bulletin 65, 272-275.
24. G. Li, V. Shrotriya, J. Huang, Y. Yao, T. Moriarty, K. Emery and Y. Yang. (2005). High-efficiency solution processable polymer photovoltaic cells by self-organization of polymer blends. Nat. Mater. 4, 864-868.
25. Q. Zhang, B. Kan, F. Liu, G. Long, X. Wan, X. Chen, Y. Zuo, W. Ni, H. Zhang, M. Li, Z. Hu, F. Huang, Y. Cao, Z. Liang, M. Zhang, T. P. Russell and Y. Chen. (2014). Small-molecule solar cells with efficiency over 9%. Nat. Photon. 9, 35-41.
26. R.-Z. Liang, Y. Zhang, V. Savikhin, M. Babics, Z. Kan, M. Wohlfahrt, N. Wehbe, S. Liu, T. Duan, M. F. Toney, F. Laquai and P. M. Beaujuge. (2019). Higher Mobility and Carrier Lifetimes in Solution-Processable Small-Molecule Ternary Solar Cells with 11% Efficiency. Adv. Energy Mater. 9, 1802836.
27. J. Zhou, Y. Zuo, X. Wan, G. Long, Q. Zhang, W. Ni, Y. Liu, Z. Li, G. He, C. Li, B. Kan, M. Li and Y. Chen. (2013). Solution-processed and high-performance organic solar cells using small molecules with a benzodithiophene unit. J. Am. Chem. Soc. 135, 8484-7.
28. B. Kan, M. Li, Q. Zhang, F. Liu, X. Wan, Y. Wang, W. Ni, G. Long, X. Yang, H. Feng, Y. Zuo, M. Zhang, F. Huang, Y. Cao, T. P. Russell and Y. Chen. (2015). A series of simple oligomer-like small molecules based on oligothiophenes for solution-processed solar cells with high efficiency. J. Am. Chem. Soc. 137, 3886-93.
29. H. Tang, H. Chen, C. Yan, J. Huang, P. W. K. Fong, J. Lv, D. Hu, R. Singh, M. Kumar, Z. Xiao, Z. Kan, S. Lu and G. Li. (2020). Delicate Morphology Control Triggers 14.7% Efficiency All-Small-Molecule Organic Solar Cells. Adv. Energy Mater. 10, 2001076.
30. J. Zhou, X. Wan, Y. Liu, Y. Zuo, Z. Li, G. He, G. Long, W. Ni, C. Li, X. Su and Y. Chen. (2012). Small molecules based on benzo[1,2-b:4,5-b']dithiophene unit for high-performance solution-processed organic solar cells. J. Am. Chem. Soc. 134, 16345-51.
31. Y. Huo, H.-L. Zhang and X. Zhan. (2019). Nonfullerene All-Small-Molecule Organic Solar Cells. ACS Energy Lett. 4, 1241-1250.
32. H. Tang, C. Yan, S. Karuthedath, H. Yin, Y. Gao, J. Gao, L. Zhang, J. Huang, S. K. So, Z. Kan, F. Laquai, G. Li and S. Lu. (2020). Deciphering the Role of Fluorination: Morphological Manipulation Prompts Charge Separation and Reduces Carrier Recombination in All-Small-Molecule Photovoltaics. Sol. RRL 4, 1900528.

33. Y. Liang, Z. Xu, J. Xia, S. T. Tsai, Y. Wu, G. Li, C. Ray and L. Yu. (2010). For the bright future-bulk heterojunction polymer solar cells with power conversion efficiency of 7.4%. Adv. Mater. 22, E135-8.
34. Y. Liang, Y. Wu, D. Feng, S. T. Tsai, H. J. Son, G. Li and L. Yu. (2009). Development of new semiconducting polymers for high performance solar cells. J. Am. Chem. Soc. 131, 56-7.
35. Y. Liang, D. Feng, Y. Wu, S. T. Tsai, G. Li, C. Ray and L. Yu. (2009). Highly efficient solar cell polymers developed via fine-tuning of structural and electronic properties. J. Am. Chem. Soc. 131, 7792-9.
36. H.-Y. Chen, J. Hou, S. Zhang, Y. Liang, G. Yang, Y. Yang, L. Yu, Y. Wu and G. Li. (2009). Polymer solar cells with enhanced open-circuit voltage and efficiency. Nat. Photon. 3, 649-653.
37. H. J. Son, B. Carsten, I. H. Jung and L. Yu. (2012). Overcoming efficiency challenges in organic solar cells: rational development of conjugated polymers. Energy & Environ. Sci. 5, 8158.
38. Y. Xu, H. Yao and J. Hou. (2019). Recent Advances in Fullerene-free Polymer Solar Cells: Materials and Devices. Chin. J. Chem. 37, 207-215.
39. S. D. Collins, N. A. Ran, M. C. Heiber and T.-Q. Nguyen. (2017). Small is Powerful: Recent Progress in Solution-Processed Small Molecule Solar Cells. Adv. Energy Mater. 7, 1602242.
40. B. Kan, Q. Zhang, M. Li, X. Wan, W. Ni, G. Long, Y. Wang, X. Yang, H. Feng and Y. Chen. (2014). Solution-processed organic solar cells based on dialkylthiol-substituted benzodithiophene unit with efficiency near 10%. J. Am. Chem. Soc. 136, 15529-32.
41. K. Sun, Z. Xiao, S. Lu, W. Zajaczkowski, W. Pisula, E. Hanssen, J. M. White, R. M. Williamson, J. Subbiah, J. Ouyang, A. B. Holmes, W. W. Wong and D. J. Jones. (2015). A molecular nematic liquid crystalline material for high-performance organic photovoltaics. Nat. Commun. 6, 6013.
42. J. Yuan, Y. Zhang, L. Zhou, G. Zhang, H.-L. Yip, T.-K. Lau, X. Lu, C. Zhu, H. Peng, P. A. Johnson, M. Leclerc, Y. Cao, J. Ulanski, Y. Li and Y. Zou. (2019). Single-Junction Organic Solar Cell with over 15% Efficiency Using Fused-Ring Acceptor with Electron-Deficient Core. Joule 3, 1140-1151.
43. J. Qin, C. An, J. Zhang, K. Ma, Y. Yang, T. Zhang, S. Li, K. Xian, Y. Cui, Y. Tang, W. Ma, H. Yao, S. Zhang, B. Xu, C. He and J. Hou. (2020). 15.3% efficiency all-small-molecule organic solar cells enabled by symmetric phenyl substitution. Sci. China Mater. 63, 1142-1150.
44. G. Li, C. W. Chu, V. Shrotriya, J. Huang and Y. Yang. (2006). Efficient inverted polymer solar cells. Appl. Phys. Lett. 88, 253503.
45. Y. Lin, Q. He, F. Zhao, L. Huo, J. Mai, X. Lu, C. J. Su, T. Li, J. Wang, J. Zhu, Y. Sun, C. Wang and X. Zhan. (2016). A Facile Planar Fused-Ring Electron Acceptor for As-Cast Polymer Solar Cells with 8.71% Efficiency. J. Am. Chem. Soc. 138, 2973-6.
46. D. Qian, Z. Zheng, H. Yao, W. Tress, T. R. Hopper, S. Chen, S. Li, J. Liu, S. Chen, J. Zhang, X. K. Liu, B. Gao, L. Ouyang, Y. Jin, G. Pozina, I. A. Buyanova, W. M. Chen, O. Inganas, V. Coropceanu, J. L. Bredas, H. Yan, J. Hou, F. Zhang, A. A. Bakulin and F. Gao. (2018). Design rules for minimizing voltage losses in high-efficiency organic solar cells. Nat. Mater. 17, 703-709.
47. S. M. Menke, N. A. Ran, G. C. Bazan and R. H. Friend. (2018). Understanding Energy Loss in Organic Solar Cells: Toward a New Efficiency Regime. Joule 2, 25-35.
48. D. Bartesaghi, C. Perez Idel, J. Kniepert, S. Roland, M. Turbiez, D. Neher and L. J. Koster. (2015). Competition between recombination and extraction of free charges determines the fill factor of organic solar cells. Nat Commun 6, 7083.

49. K. Gao, S. B. Jo, X. Shi, L. Nian, M. Zhang, Y. Kan, F. Lin, B. Kan, B. Xu, Q. Rong, L. Shui, F. Liu, X. Peng, G. Zhou, Y. Cao and A. K. Y. Jen. (2019). Over 12% Efficiency Nonfullerene All-Small-Molecule Organic Solar Cells with Sequentially Evolved Multilength Scale Morphologies. Adv. Mater. 31, 1807842.
50. R.-Z. Liang, M. Babics, A. Seitkhan, K. Wang, P. B. Geraghty, S. Lopatin, F. Cruciani, Y. Firdaus, M. Caporuscio, D. J. Jones and P. M. Beaujuge. (2018). Additive-Morphology Interplay and Loss Channels in "All-Small-Molecule" Bulk-heterojunction (BHJ) Solar Cells with the Nonfullerene Acceptor IDTTBM. Adv. Func. Mater. 28, 1705464.
51. H. Yin, L. K. Ma, Y. Wang, J. Huang, H. Yu, J. Zhang, P. C. Y. Chow, W. Ma, S. K. So and H. Yan. (2019). Donor Polymer Can Assist Electron Transport in Bulk Heterojunction Blends with Small Energetic Offsets. Adv. Mater. 30, 1903998.
52. J. Huang, L. Xie, L. Hong, L. Wu, Y. Han, T. Yan, J. Zhang, L. Zhu, Z. Wei and Z. Ge. (2019). Significant influence of halogenation on the energy levels and molecular configurations of polymers in DTBDT-based polymer solar cells. Mater. Chem. Front. 3, 1244-1252.
53. D. Deng, Y. Zhang, J. Zhang, Z. Wang, L. Zhu, J. Fang, B. Xia, Z. Wang, K. Lu, W. Ma and Z. Wei. (2016). Fluorination-enabled optimal morphology leads to over 11% efficiency for inverted small-molecule organic solar cells. Nat. Commun. 7, 13740.
54. J. Wan, X. Xu, G. Zhang, Y. Li, K. Feng and Q. Peng. (2017). Highly efficient halogen-free solvent processed small-molecule organic solar cells enabled by material design and device engineering. Energy & Environ. Sci. 10, 1739-1745.
55. H. Sun, T. Liu, J. Yu, T.-K. Lau, G. Zhang, Y. Zhang, M. Su, Y. Tang, R. Ma, B. Liu, J. Liang, K. Feng, X. Lu, X. Guo, F. Gao and H. Yan. (2019). A monothiophene unit incorporating both fluoro and ester substitution enabling high-performance donor polymers for non-fullerene solar cells with 16.4% efficiency. Energy & Environ. Sci. 12, 3328-3337.
56. H. Bin, Y. Yang, Z. G. Zhang, L. Ye, M. Ghasemi, S. Chen, Y. Zhang, C. Zhang, C. Sun, L. Xue, C. Yang, H. Ade and Y. Li. (2017). 9.73% Efficiency Nonfullerene All Organic Small Molecule Solar Cells with Absorption-Complementary Donor and Acceptor. J. Am. Chem. Soc. 139, 5085-5094.
57. T. Duan, J. Gao, T. Xu, Z. Kan, W. Chen, R. Singh, G. P. Kini, C. Zhong, D. Yu, Z. Xiao, Z. Xiao and S. Lu. (2020). Simple organic donors based on halogenated oligothiophenes for all small molecule solar cells with efficiency over 11%. J. Mater. Chem. A 8, 5843-5847.
58. H. Li, Q. Wu, R. Zhou, Y. Shi, C. Yang, Y. Zhang, J. Zhang, W. Zou, D. Deng, K. Lu and Z. Wei. (2018). Liquid-Crystalline Small Molecules for Nonfullerene Solar Cells with High Fill Factors and Power Conversion Efficiencies. Adv. Energy Mater. 9, 1803175.
59. Y. Huang, W. Wen, S. Mukherjee, H. Ade, E. J. Kramer and G. C. Bazan. (2014). High-molecular-weight insulating polymers can improve the performance of molecular solar cells. Adv. Mater. 26, 4168-72.
60. S. Badgujar, G.-Y. Lee, T. Park, C. E. Song, S. Park, S. Oh, W. S. Shin, S.-J. Moon, J.-C. Lee and S. K. Lee. (2016). High-Performance Small Molecule via Tailoring Intermolecular Interactions and its Application in Large-Area Organic Photovoltaic Modules. Adv. Energy Mater. 6, 1600228.
61. S. Zhang, L. Yang, D. Liu, C. He, J. Zhang, Y. Zhang and J. Hou. (2017). Influence of the replacement of alkoxyl with alkylthienyl on photovoltaic properties of two small molecule donors for organic solar cells. Sci. China Chem. 60, 1340-1348.

62. L. Yang, S. Zhang, C. He, J. Zhang, Y. Yang, J. Zhu, Y. Cui, W. Zhao, H. Zhang, Y. Zhang, Z. Wei and J. Hou. (2018). Modulating Molecular Orientation Enables Efficient Nonfullerene Small-Molecule Organic Solar Cells. Chem. Mater. 30, 2129-2134.
63. S. Badgujar, C. E. Song, S. Oh, W. S. Shin, S.-J. Moon, J.-C. Lee, I. H. Jung and S. K. Lee. (2016). Highly efficient and thermally stable fullerene-free organic solar cells based on a small molecule donor and acceptor. J. Mater. Chem. A 4, 16335-16340.
64. B. Qiu, L. Xue, Y. Yang, H. Bin, Y. Zhang, C. Zhang, M. Xiao, K. Park, W. Morrison, Z.-G. Zhang and Y. Li. (2017). All-Small-Molecule Nonfullerene Organic Solar Cells with High Fill Factor and High Efficiency over 10%. Chem. Mater. 29, 7543-7553.
65. R. Xin, J. Feng, C. Zeng, W. Jiang, L. Zhang, D. Meng, Z. Ren, Z. Wang and S. Yan. (2017). Nonfullerene-Acceptor All-Small-Molecule Organic Solar Cells Based on Highly Twisted Perylene Bisimide with an Efficiency of over 6. ACS Appl. Mater. Interfaces 9, 2739-2746.
66. R.-Z. Liang, M. Babics, V. Savikhin, W. Zhang, V. M. Le Corre, S. Lopatin, Z. Kan, Y. Firdaus, S. Liu, I. McCulloch, M. F. Toney and P. M. Beaujuge. (2018). Carrier Transport and Recombination in Efficient "All-Small-Molecule" Solar Cells with the Nonfullerene Acceptor IDTBR. Adv. Energy Mater. 8, 1800264.
67. T. Duan, H. Tang, R.-Z. Liang, J. Lv, Z. Kan, R. Singh, M. Kumar, Z. Xiao, S. Lu and F. Laquai. (2019). Terminal group engineering for small-molecule donors boosts the performance of nonfullerene organic solar cells. J. Mater. Chem. A 7, 2541-2546.
68. Y. Liu, C. C. Chen, Z. Hong, J. Gao, Y. M. Yang, H. Zhou, L. Dou, G. Li and Y. Yang. (2013). Solution-processed small-molecule solar cells: breaking the 10% power conversion efficiency. Sci. Rep. 3, 3356.
69. H. Bin, J. Yao, Y. Yang, I. Angunawela, C. Sun, L. Gao, L. Ye, B. Qiu, L. Xue, C. Zhu, C. Yang, Z. G. Zhang, H. Ade and Y. Li. (2018). High-Efficiency All-Small-Molecule Organic Solar Cells Based on an Organic Molecule Donor with Alkylsilyl-Thienyl Conjugated Side Chains. Adv. Mater. 30, 1706361.
70. J. Guo, H. Bin, W. Wang, B. Chen, J. Guo, R. Sun, Z.-G. Zhang, X. Jiao, Y. Li and J. Min. (2018). All-small molecule solar cells based on donor molecule optimization with highly enhanced efficiency and stability. J. Mater. Chem. A 6, 15675-15683.
71. Y. Lin, J. Wang, T. Li, Y. Wu, C. Wang, L. Han, Y. Yao, W. Ma and X. Zhan. (2016). Efficient fullerene-free organic solar cells based on fused-ring oligomer molecules. J. Mater. Chem. A 4, 1486-1494.
72. Y. Huo, J. Zhu, X.-Z. Wang, C. Yan, Y.-F. Chai, Z.-Z. Chen, X. Zhan and H.-L. Zhang. (2018). Small molecule donors based on benzodithiophene and diketopyrrolopyrrole compatible with both fullerene and non-fullerene acceptors. J. Mater. Chem. C 6, 5843-5848.
73. J. Min, C. Cui, T. Heumueller, S. Fladischer, X. Cheng, E. Spiecker, Y. Li and C. J. Brabec. (2016). Side-Chain Engineering for Enhancing the Properties of Small Molecule Solar Cells: A Trade-off Beyond Efficiency. Adv. Energy Mater. 6, 1600515.
74. J. Min, O. K. Kwon, C. Cui, J.-H. Park, Y. Wu, S. Y. Park, Y. Li and C. J. Brabec. (2016). High performance all-small-molecule solar cells: engineering the nanomorphology via processing additives. J. Mater. Chem. A 4, 14234-14240.
75. B. Kan, Q. Zhang, F. Liu, X. Wan, Y. Wang, W. Ni, X. Yang, M. Zhang, H. Zhang, T. P. Russell and Y. Chen. (2015). Small Molecules Based on Alkyl/Alkylthio-thieno[3,2-b]thiophene-Substituted Benzo[1,2-b:4,5-b′]dithiophene for Solution-Processed Solar Cells with High Performance. Chem. Mater. 27, 8414-8423.

76. H. Chen, D. Hu, Q. Yang, J. Gao, J. Fu, K. Yang, H. He, S. Chen, Z. Kan, T. Duan, C. Yang, J. Ouyang, Z. Xiao, K. Sun and S. Lu. (2019). All-Small-Molecule Organic Solar Cells with an Ordered Liquid Crystalline Donor. Joule 3, 3034-3047.
77. H. Tang, T. Xu, C. Yan, J. Gao, H. Yin, J. Lv, R. Singh, M. Kumar, T. Duan, Z. Kan, S. Lu and G. Li. (2019). Donor Derivative Incorporation: An Effective Strategy toward High Performance All-Small-Molecule Ternary Organic Solar Cells. Adv. Sci. 6, 1901613.
78. C. J. Lee, V. D. Mitchell, J. White, X. Jiao, C. R. McNeill, J. Subbiah and D. J. Jones. (2019). Solubilizing core modifications on high-performing benzodithiophene-based molecular semiconductors and their influences on film nanostructure and photovoltaic performance. J. Mater. Chem. A 7, 6312-6326.
79. J. Ge, L. Xie, R. Peng, B. Fanady, J. Huang, W. Song, T. Yan, W. Zhang and Z. Ge. (2020). 13.34 % Efficiency Non-Fullerene All-Small-Molecule Organic Solar Cells Enabled by Modulating the Crystallinity of Donors via a Fluorination Strategy. Angew. Chem. Int. Ed. 59, 2808-2815.
80. X. Dong, K. Yang, H. Tang, D. Hu, S. Chen, J. Zhang, Z. Kan, T. Duan, C. Hu, X. Dai, Z. Xiao, K. Sun and S. Lu. (2019). Improving Molecular Planarity by Changing Alky Chain Position Enables 12.3% Efficiency All-Small-Molecule Organic Solar Cells with Enhanced Carrier Lifetime and Reduced Recombination. Sol. RRL 4, 1900326.
81. H. Wu, H. Fan, S. Xu, L. Ye, Y. Guo, Y. Yi, H. Ade and X. Zhu. (2019). Isomery-Dependent Miscibility Enables High-Performance All-Small-Molecule Solar Cells. Small 15, 1804271.
82. H. Wu, H. Fan, W. Liu, S. Chen, C. Yang, L. Ye, H. Ade and X. Zhu. (2019). Conjugation-Curtailing of Benzodithionopyran-Cored Molecular Acceptor Enables Efficient Air-Processed Small Molecule Solar Cells. Small 15, 1902656.
83. Q. Yue, H. Wu, Z. Zhou, M. Zhang, F. Liu and X. Zhu. (2019). 13.7% Efficiency Small-Molecule Solar Cells Enabled by a Combination of Material and Morphology Optimization. Adv. Mater. 31, 1904283.
84. H. Wu, Q. Yue, Z. Zhou, S. Chen, D. Zhang, S. Xu, H. Zhou, C. Yang, H. Fan and X. Zhu. (2019). Cathode interfacial layer-free all small-molecule solar cells with efficiency over 12%. J. Mater. Chem. A 7, 15944-15950.
85. B. Qiu, S. Chen, L. Xue, C. Sun, X. Li, Z. G. Zhang, C. Yang and Y. Li. (2018). Effects of Alkoxy and Fluorine Atom Substitution of Donor Molecules on the Morphology and Photovoltaic Performance of All Small Molecule Organic Solar Cells. Front Chem. 6, 413.
86. J. Gao, J. Ge, R. Peng, C. Liu, L. Cao, D. Zhang, B. Fanady, L. Hong, E. Zhou and Z. Ge. (2020). Over 14% efficiency nonfullerene all-small-molecule organic solar cells enabled by improving the ordering of molecular donors via side-chain engineering. J. Mater. Chem. A 8, 7405-7411.
87. J. Huang, X. Wang, X. Zhang, Z. Niu, Z. Lu, B. Jiang, Y. Sun, C. Zhan and J. Yao. (2014). Additive-assisted control over phase-separated nanostructures by manipulating alkylthienyl position at donor backbone for solution-processed, non-fullerene, all-small-molecule solar cells. ACS Appl. Mater. Interfaces 6, 3853-62.
88. Y. Huo, X.-T. Gong, T.-K. Lau, T. Xiao, C. Yan, X. Lu, G. Lu, X. Zhan and H.-L. Zhang. (2018). Dual-Accepting-Unit Design of Donor Material for All-Small-Molecule Organic Solar Cells with Efficiency Approaching 11%. Chem. Mater. 30, 8661-8668.

89. Q. Wu, D. Deng, J. Zhang, W. Zou, Y. Yang, Z. Wang, H. Li, R. Zhou, K. Lu and Z. Wei. (2019). Fluorination-substitution effect on all-small-molecule organic solar cells. Sci. China Chem. 62, 837-844.
90. M. A. Adil, J. Zhang, D. Deng, Z. Wang, Y. Yang, Q. Wu and Z. Wei. (2018). Modulation of the Molecular Orientation at the Bulk Heterojunction Interface via Tuning the Small Molecular Donor-Nonfullerene Acceptor Interactions. ACS Appl. Mater. Interfaces 10, 31526-31534.
91. C. Yan, T. Liu, Y. Chen, R. Ma, H. Tang, G. Li, T. Li, Y. Xiao, T. Yang, X. Lu, X. Zhan, H. Yan, G. Li and B. Tang. (2019). ITC-2Cl: a Versatile Middle-Bandgap Nonfullerene Acceptor for High-Efficiency Panchromatic Ternary Organic Solar Cells. Sol. RRL 3, 201900377.
92. J. Gao, W. Chen, L. Dou, C.-C. Chen, W.-H. Chang, Y. Liu, G. Li and Y. Yang. (2014). Elucidating Double Aggregation Mechanisms in the Morphology Optimization of Diketopyrrolopyrrole-Based Narrow Bandgap Polymer Solar Cells. Adv. Mater. 26, 3142–3147.
93. H. Yin, K. L. Chiu, P. Bi, G. Li, C. Yan, H. Tang, C. Zhang, Y. Xiao, H. Zhang, W. Yu, H. Hu, X. Lu, X. Hao and S. K. So. (2019). Enhanced Electron Transport and Heat Transfer Boost Light Stability of Ternary Organic Photovoltaic Cells Incorporating Non-Fullerene Small Molecule and Polymer Acceptors. Adv. Electron. Mater. 5, 1900497.
94. R. Sun, Y. Wu, J. Guo, Z. Luo, C. Yang and J. Min. (2020). High-efficiency all-small-molecule organic solar cells based on an organic molecule donor with an asymmetric thieno[2,3-f] benzofuran unit. Sci. China Chem. DOI: 10.1007/s11426-020-9753-x
95. L. Yuan, Y. Zhao, J. Zhang, Y. Zhang, L. Zhu, K. Lu, W. Yan and Z. Wei. (2015). Oligomeric Donor Material for High-Efficiency Organic Solar Cells: Breaking Down a Polymer. Adv. Mater. 27, 4229-33.
96. B. Qiu, Z. Chen, S. Qin, J. Yao, W. Huang, L. Meng, H. Zhu, Y. M. Yang, Z. G. Zhang and Y. Li. (2020). Highly Efficient All-Small-Molecule Organic Solar Cells with Appropriate Active Layer Morphology by Side Chain Engineering of Donor Molecules and Thermal Annealing. Adv. Mater. 32, 1908373.
97. Z. Zhou, S. Xu, J. Song, Y. Jin, Q. Yue, Y. Qian, F. Liu, F. Zhang and X. Zhu. (2018). High-efficiency small-molecule ternary solar cells with a hierarchical morphology enabled by synergizing fullerene and non-fullerene acceptors. Nat. Energy 3, 952-959.
98. Y. Chang, Y. Chang, X. Zhu, X. Zhou, C. Yang, J. Zhang, K. Lu, X. Sun and Z. Wei. (2019). Constructing High-Performance All-Small-Molecule Ternary Solar Cells with the Same Third Component but Different Mechanisms for Fullerene and Non-fullerene Systems. Adv. Energy Mater. 9, 1900190.
99. Q. Fan, T. Liu, M. Zhang, W. Su, U. A. Méndez-Romero, T. Yang, X. Geng, L. Hou, D. Yu, F. Liu, H. Yan and E. Wang. (2020). Weak Makes It Powerful: The Role of Cognate Small Molecules as an Alloy Donor in 2D/1A Ternary Fullerene Solar Cells for Finely Tuned Hierarchical Morphology in Thick Active Layers. Small Methods 4, 1900766.
100. Z. Wang, X. Zhu, J. Zhang, K. Lu, J. Fang, Y. Zhang, Z. Wang, L. Zhu, W. Ma, Z. Shuai and Z. Wei. (2018). From Alloy-Like to Cascade Blended Structure: Designing High-Performance All-Small-Molecule Ternary Solar Cells. J. Am. Chem. Soc. 140, 1549-1556.
101. M. Zhang, J. Wang, F. Zhang, Y. Mi, Q. An, W. Wang, X. Ma, J. Zhang and X. Liu. (2017). Ternary small molecule solar cells exhibiting power conversion efficiency of 10.3%. Nano Energy 39, 571-581.
102. H. Zhang, X. Wang, L. Yang, S. Zhang, Y. Zhang, C. He, W. Ma and J. Hou. (2017). Improved Domain Size and Purity Enables Efficient All-Small-Molecule Ternary Solar Cells. Adv. Mater. 29, 1703777.

103. C. Xu, J. Wang, Q. An, X. Ma, Z. Hu, J. Gao, J. Zhang and F. Zhang. (2019). Ternary small molecules organic photovoltaics exhibiting 12.84% efficiency. Nano Energy 66, 104119.
104. D. Hu, Q. Yang, H. Chen, F. Wobben, V. M. Le Corre, R. Singh, T. Liu, R. Ma, H. Tang, L. J. A. Koster, T. Duan, H. Yan, Z. Kan, Z. Xiao and S. Lu. (2020). 15.34% efficiency all-small-molecule organic solar cells with an improved fill factor enabled by a fullerene additive. Energy & Environ. Sci. 13, 2134-2141.
105. H. Yin, C. Zhang, H. Hu, S. Karuthedath, Y. Gao, H. Tang, C. Yan, L. Cui, P. W. K. Fong, Z. Zhang, Y. Gao, J. Yang, Z. Xiao, L. Ding, F. Laquai, S. K. So and G. Li. (2019). Highly Crystalline Near-Infrared Acceptor Enabling Simultaneous Efficiency and Photostability Boosting in High-Performance Ternary Organic Solar Cells. ACS Appl. Mater. Interfaces 11, 48095-48102.
106. Y. Yang, W. Chen, L. Dou, W.-H. Chang, H.-S. Duan, B. Bob, G. Li and Y. Yang. (2015). High-performance multiple-donor bulk heterojunction solar cells. Nat. Photon. 9, 190-198.
107. P. Cheng and X. Zhan. (2015). Versatile third components for efficient and stable organic solar cells. Mater. Horiz. 2, 462-485.
108. L. Zhan, S. Li, T.-K. Lau, Y. Cui, X. Lu, M. Shi, C.-Z. Li, H. Li, J. Hou and H. Chen. (2020). Over 17% efficiency ternary organic solar cells enabled by two non-fullerene acceptors working in an alloy-like model. Energy & Environ. Sci. 13, 635-645.
109. T. Liu, Z. Luo, Q. Fan, G. Zhang, L. Zhang, W. Gao, X. Guo, W. Ma, M. Zhang, C. Yang, Y. Li and H. Yan. (2018). Use of two structurally similar small molecular acceptors enabling ternary organic solar cells with high efficiencies and fill factors. Energy & Environ. Sci. 11, 3275-3282.
110. T. Liu, Z. Luo, Y. Chen, T. Yang, Y. Xiao, G. Zhang, R. Ma, X. Lu, C. Zhan, M. Zhang, C. Yang, Y. Li, J. Yao and H. Yan. (2019). A nonfullerene acceptor with a 1000 nm absorption edge enables ternary organic solar cells with improved optical and morphological properties and efficiencies over 15%. Energy & Environ. Sci. 12, 2529--2536.
111. C. Yan, H. Tang, R. Ma, M. Zhang, T. Liu, J. Lv, J. Huang, Y. Yang, T. Xu, Z. Kan, H. Yan, F. Liu, S. Lu and G. Li. (2020). Synergy of Liquid-Crystalline Small-Molecule and Polymeric Donors Delivers Uncommon Morphology Evolution and 16.6% Efficiency Organic Photovoltaics. Adv. Sci. 7, 2000149.
112. Q. An, J. Wang, W. Gao, X. Ma, Z. Hu, J. Gao, C. Xu, M. Hao, X. Zhang, C. Yang and F. Zhang. (2020). Alloy-like ternary polymer solar cells with over 17.2% efficiency. Science Bulletin 65, 538-545.
113. J. Lv, Y. Feng, J. Fu, J. Gao, R. Singh, M. Kumar, M. Kim, H. Tang, S. Lu, W. Zhang, I. McCulloch, J. Li and Z. Kan. (2019). Energetic Disorder and Activation Energy in Efficient Ternary Organic Solar Cells with Nonfullerene Acceptor Eh-IDTBR as the Third Component. Sol. RRL 4, 1900403.
114. T. Ameri, P. Khoram, J. Min and C. J. Brabec. (2013). Organic ternary solar cells: a review. Adv. Mater. 25, 4245-66.

Graphical Abstract

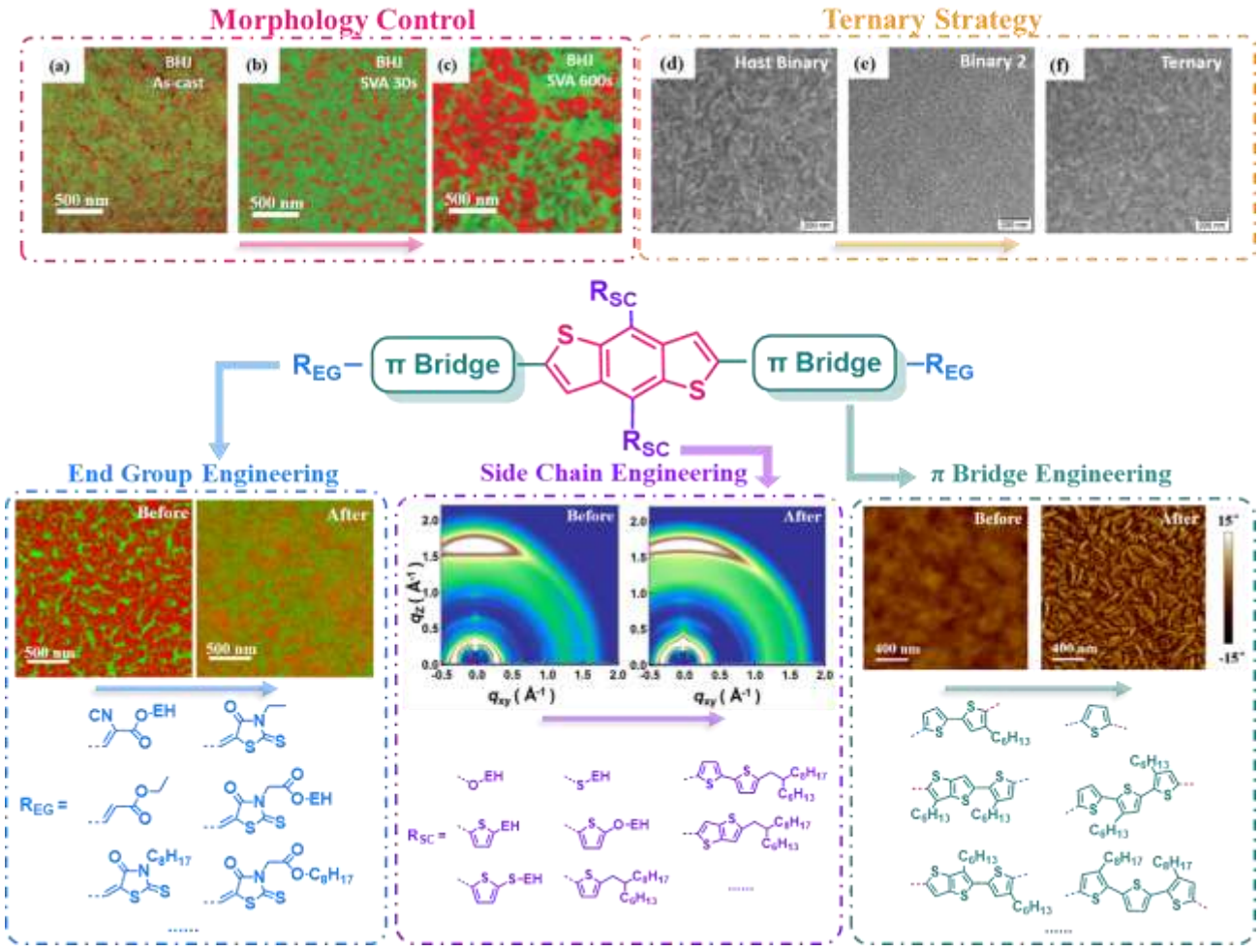

Progress and Potential

All-small-molecule (ASM) organic solar cells (OSCs) have been of academic interests for decades owing to the unique superiorities of small molecules, such as well-defined structures, easy purification, and excellent batch-to-batch replicability. However, they received little attention prior to 2011 due to rather disappointing device performance. Since 2011, the photovoltaic performance of ASM OSCs have been rapidly elevated due to the advance of Benzodithiophene (BDT)-based small molecule donors, and in particular, with the latest small

molecule acceptors, over 15% benchmark efficiency has been obtained in the laboratory, which brings potential towards commercialization. In this light, the ASM OSCs based on BDT small molecule donors are considered being a promising candidate for next-generation photovoltaic technology to deliver cost–effective, versatile form-factor/application and environmental-friendly energy.